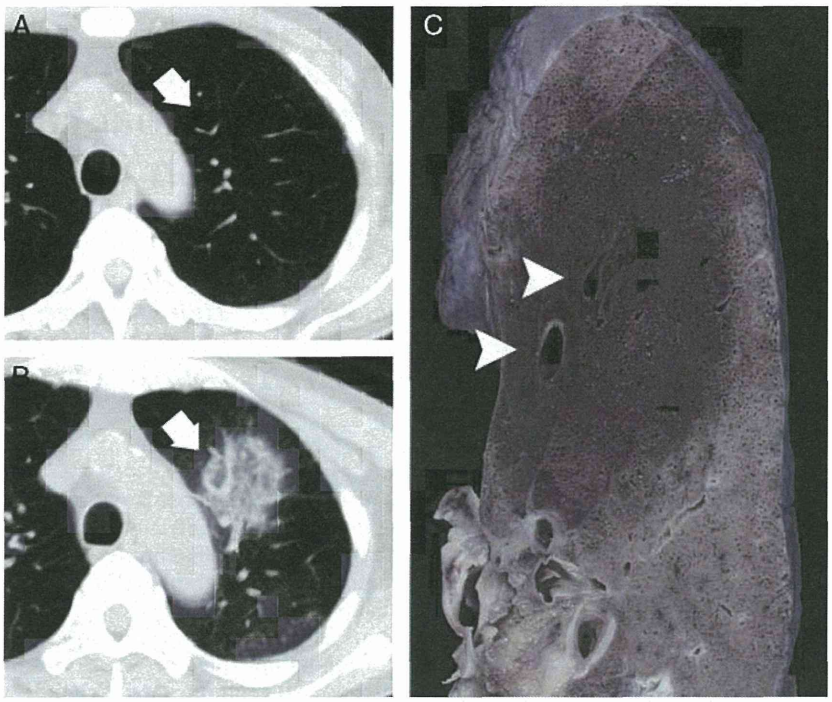

FIGURE 1. Irregular pulmonary vein dilation (case 1). A, Chest CT scan taken 8 months before the last admission shows normal pulmonary veins (arrow) in the upper lobe of the left lung. B, Chest CT scan taken during the last admission shows irregular pulmonary vein dilation (arrow) surrounded by ground-glass opacity. C, Pulmonary venous invasion is surrounded by hemorrhage at autopsy (arrowheads).

fungal hyphae invading the pulmonary veins and arteries, which resulted in hemorrhagic infarction of the lung.

Case 3

A 64-year-old man with overt leukemia from myelodysplastic syndrome developed a high-grade fever above 38°C, and his chest x-ray and chest CT scan revealed small nodules in the lungs bilaterally. His WBC count was 900/mm^3, and 36% of blastocytes was revealed. Serum *Aspergillus* galactomannan antigen was negative. After a 2-week course of voriconazole, a follow-up CT scan showed an increasing number of small nodules along with irregular dilation of the pulmonary veins in the right lung, compared with the CT at admission (Fig. 4). Despite treatment with amphotericin-B, right maxillary sinusitis developed, and progressive respiratory failure caused his death. At autopsy, fungal hyphae were found to have invaded the pulmonary vessels and bronchi, which resulted in massive hemorrhagic pulmonary infarction.

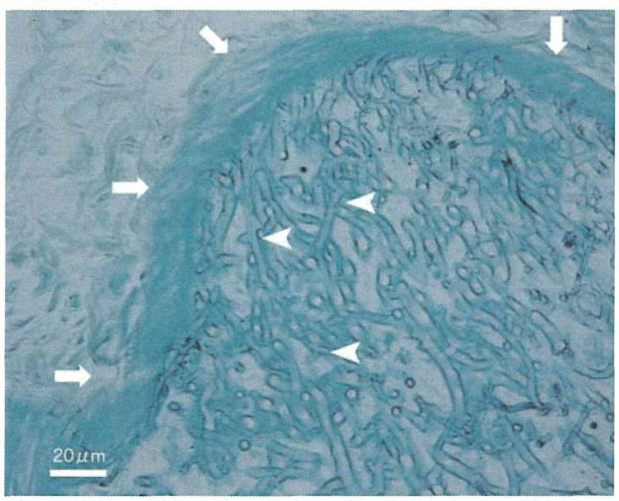

FIGURE 2. Spreading broad aseptate fungal hyphae in the pulmonary vein at autopsy of case 1 (Grocott's Methenamine Silver stain, ×400). The pulmonary vein and typical right-angle branching of the hyphae are indicated by arrows and arrowheads, respectively.

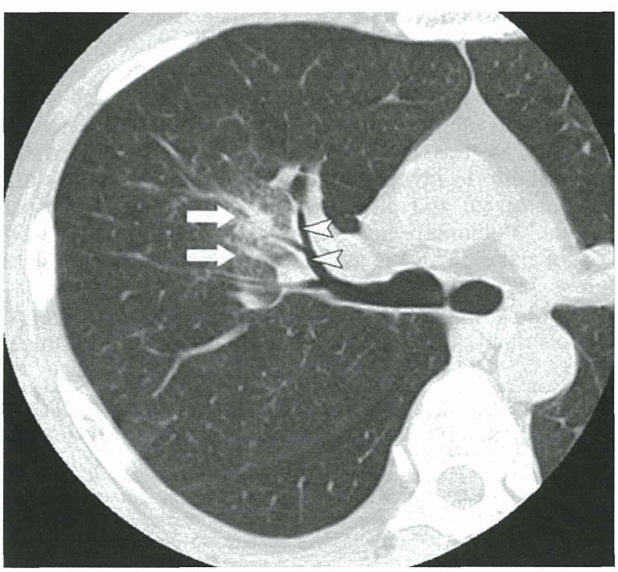

FIGURE 3. Irregular pulmonary vein dilation (case 2): chest CT scan taken during the last admission shows bronchial wall thickening (arrowhead) and irregular pulmonary vein dilation (arrows) surrounded by ground-glass opacity.

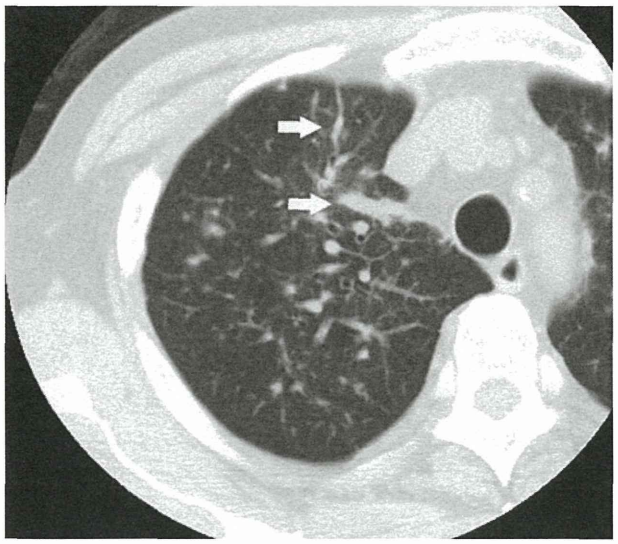

FIGURE 4. Irregular pulmonary vein dilation (case 3): chest CT scan taken 2 weeks after the last admission shows irregular pulmonary vein dilation (arrows) and increasing small nodules.

DISCUSSION

Although zygomycosis is the third most prevalent cause of fungal infection after aspergillosis and candidiasis, it is important to consider zygomycotic infection in patients with immunocompromised status or hematological disorders because of its high mortality rate.[2] Invasive aspergillosis is the most important differential diagnosis of zygomycosis. Radiologically, pleural effusion and pulmonary artery pseudoaneurysm are characteristic features of zygomycosis and are useful to distinguish between the 2 diseases[3,6]; however, these findings are thought to emerge in the advanced stages of disease and to be rare.[6] In the cases reviewed here, chest CT scans showed irregular dilation of the pulmonary veins, which proved the invasion by fungal hyphae on autopsy. As these changes preceded the hemorrhagic brain infarction (case 1), pleural effusion, and consolidation (cases 2 and 3), they can be regarded as earlier and more frequent indicators of zygomycosis. There may be several reasons why the development of venous invasion occurs in the earlier stages of zygomycosis. First, the pulmonary vein does not have a thick elastic layer compared with the pulmonary artery. Second, as the venous blood is better oxygenized than the arterial blood in the lung, the fungi may be able to invade easily and grow fast in the pulmonary veins. Thus, it is reasonable that the pulmonary venous finding may help to make an earlier decision for invasive diagnostic procedures or immediate treatment.

Circulating levels of galactomannan *Aspergillus* antigen are known to be a useful tool for the distinction between zygomycosis and invasive aspergillosis. When the test result is negative, it is highly unlikely that the diagnosis is invasive aspergillosis.[7] We observed a negative result for serum galactomannan *Aspergillus* antigen, and also decreased neutrophils and use of azole antifungal agents along with sinusitis or deferoxamine intake. This evidence strengthens the conclusion that combining the negative *Aspergillus* antigen result with other clinical information may be beneficial for the diagnosis of zygomycosis. Early diagnosis based on these characteristic findings can contribute to curative operation, adequate antifungal medication,[8] and the determination of involvement of other organs.[4] However, because this study included only 3 cases of zygomycosis, analyses of more cases are needed to verify these radiologic and clinical findings.

In summary, we report 3 cases of pulmonary zygomycosis occurring in patients with hematological diseases. Irregular pulmonary venous dilation on chest CT corresponds with autopsy findings of fungal angioinvasion. In addition to recognition of these characteristic CT findings, assessment of characteristic clinical risk factors may be useful for physicians to suspect the possibility of zygomycosis in order to contribute to earlier diagnosis, more successful treatment, and better clinical outcome.

ACKNOWLEDGMENT

The authors thank the NIH Fellows Editorial Board for reviewing the manuscript.

REFERENCES

1. Pagano L, Ricci P, Tonso A, et al. Mucormycosis in patients with haematological malignancies: a retrospective clinical study of 37 cases. *Br J Haematol.* 1997;99:331–336.
2. Chayakulkeeree M, Ghannoum MA, Perfect JR. Zygomycosis: the re-emerging fungal infection. *Eur J Clin Microbiol Infect Dis.* 2006;25:215–229.
3. Chamilos G, Marom EM, Lewis RE, et al. Predictors of pulmonary zygomycosis versus invasive pulmonary aspergillosis in patients with cancer. *Clinical Infectious Diseases.* 2005;41:60–66.
4. Roden MM, Zaoutis TE, Buchanan WL, et al. Epidemiology and outcome of zygomycosis: a review of 929 reported cases. *Clin Infect Dis.* 2005;41:634–653.
5. Won HJ, Lee KS, Cheon JE, et al. Invasive pulmonary aspergillosis: prediction at thin-section CT in patients with neutropenia—a prospective study. *Radiology.* 1998;208:777–782.
6. McAdams HP, Rosado de Christenso M, Strollo DC, et al. Pulmonary mucormycosis: radiologic findings in 32 cases. *Am J Roentgenol.* 1997;168:1541–1548.
7. Maertens J, Verhaegen J, Lagrou K, et al. Screening for circulating galactomannan as a noninvasive diagnostic tool for invasive aspergillosis in prolonged neutropenic patients and stem cell transplantation recipients: a prospective validation. *Blood.* 2001;97:1604–1610.
8. Gonzalez CE, Couriel DR, Walsh TJ. Disseminated zygomycosis in a neutropenic patient: successful treatment with amphotericin B lipid complex and granulocyte colony-stimulating factor. *Clin Infect Dis.* 1997;24:192–196.

OPEN ACCESS Freely available online

PLoS one

Quantitative Analysis of Viral Load per Haploid Genome Revealed the Different Biological Features of Merkel Cell Polyomavirus Infection in Skin Tumor

Satoshi Ota[1,2], Shumpei Ishikawa[2]*, Yutaka Takazawa[2], Akiteru Goto[2], Takeshi Fujii[3], Ken-ichi Ohashi[3], Masashi Fukayama[2]

1 Department of Pathology, Chiba University Hospital, University of Chiba, Chuo, Chiba, Chiba, Japan, **2** Department of Pathology, Graduate School of Medicine, University of Tokyo, Bunkyo, Tokyo, Japan, **3** Department of Pathology, Toranomon Hospital, Minato, Tokyo, Japan

Abstract

Merkel cell polyomavirus (MCPyV) has recently been identified in Merkel cell carcinoma (MCC), an aggressive cancer that occurs in sun-exposed skin. Conventional technologies, such as polymerase chain reaction (PCR) and immunohistochemistry, have produced conflicting results for MCPyV infections in non-MCC tumors. Therefore, we performed quantitative analyses of the MCPyV copy number in various skin tumor tissues, including MCC (n = 9) and other sun exposure-related skin tumors (basal cell carcinoma [BCC, n = 45], actinic keratosis [AK, n = 52], Bowen's disease [n = 34], seborrheic keratosis [n = 5], primary cutaneous anaplastic large-cell lymphoma [n = 5], malignant melanoma [n = 5], and melanocytic nevus [n = 6]). In a conventional PCR analysis, MCPyV DNA was detected in MCC (9 cases; 100%), BCC (1 case; 2%), and AK (3 cases; 6%). We then used digital PCR technology to estimate the absolute viral copy number per haploid human genome in these tissues. The viral copy number per haploid genome was estimated to be around 1 in most MCC tissues, and there were marked differences between the MCC (0.119–42.8) and AK (0.02–0.07) groups. PCR-positive BCC tissue showed a similar viral load as MCC tissue (0.662). Immunohistochemistry with a monoclonal antibody against the MCPyV T antigen (CM2B4) demonstrated positive nuclear localization in most of the high-viral-load tumor groups (8 of 9 MCC and 1 BCC), but not in the low-viral-load or PCR-negative tumor groups. These results demonstrated that MCPyV infection is possibly involved in a minority of sun-exposed skin tumors, including BCC and AK, and that these tumors display different modes of infection.

Citation: Ota S, Ishikawa S, Takazawa Y, Goto A, Fujii T, et al. (2012) Quantitative Analysis of Viral Load per Haploid Genome Revealed the Different Biological Features of Merkel Cell Polyomavirus Infection in Skin Tumor. PLoS ONE 7(6): e39954. doi:10.1371/journal.pone.0039954

Editor: Amanda Ewart Toland, Ohio State University Medical Center, United States of America

Received January 10, 2012; **Accepted** May 29, 2012; **Published** June 29, 2012

Funding: This study was supported by the Industrial Technology Research Grant Program of the New Energy and Industrial Technology Development Organization (NEDO) of Japan (S.I.) and Grants-in-Aid for Scientific Research on Innovative Areas from the Ministry of Education, Culture, Sports, Science and Technology of Japan (S.I.). The funders had no role in study design, data collection and analysis, decision to publish, or preparation of the manuscript.

Competing Interests: The authors have declared that no competing interests exist.

* E-mail: isikawas-tky@umin.org

Introduction

Merkel cell carcinoma (MCC), which is a rare and aggressive primary cutaneous neoplasm that affects elderly and/or immunocompromised individuals, tends to occur in sun-exposed skin [1]. The Merkel cell polyomavirus (MCPyV) was recently identified in MCC [2], and its frequency in MCC has been reported to be 100% by immunohistochemical and/or polymerase chain reaction (PCR) studies that were performed in western countries [2–23] and in East Asia [24–27]. The monoclonal integration of MCPyV DNA in host DNA has been demonstrated in neoplastic MCC cells, indicating that the virus causes and/or promotes this specific type of cutaneous neoplasm [2]. However, it remains unclear how often MCPyV is associated with other cutaneous neoplasms and to what extent racial factors influence the infection rates. In skin tumors other than MCC, MCPyV has been detected at various frequencies (0%–25%) by PCR. However, immunohistochemical analyses have suggested that MCPyV is specific to MCC and is absent from other skin tumors, including squamous cell carcinoma, basal cell carcinoma (BCC), and lymphoma [28,29]. MCPyV T-antigen expression may be suppressed in infected cells in certain circumstances, even though MCPyV viral DNA is integrated into the cellular DNA. A significant number of MCPyV-positive cases are positive for the small-T (ST) antigen but do not express the large-T (LT) antigen [30]. Recently, Neumann et al. found that all integrated genomes had truncation mutations in the LT antigen [31]. However, it may be difficult to address these issues without a sensitive quantitative detection method.

In the present study, we investigated the frequency of MCPyV infection in skin tumors, including MCC and other sun exposure-related skin tumors, such as BCC, actinic keratosis (AK), and Bowen's disease (BD), in Japan. Other representative non-melanocytic, melanocytic, and lymphoid skin tumors were also included. We applied digital PCR in order to calculate the absolute viral copy number per haploid human genome [32,33]. This method uses nanofluidic technology to randomly distribute applied DNA molecules to multiple small reaction chambers at a concentration of 0 to 1 DNA molecules per chamber. Target and reference genes are simultaneously PCR-amplified with a dual-color amplification reaction, and their copy numbers are then calculated by counting the numbers of signal-positive chambers. This PCR-efficiency-independent method is highly robust for comparing copy numbers using different primer sets. The results

we obtained for viral load using this quantitative method revealed the different biological characteristics of MCPyV in these tumors and provided a reasonable explanation for the conflicting results obtained so far.

Results

Diagnosis of MCC

The diagnosis of MCC was confirmed by the presence of a perinuclear dot-like positive staining pattern for CK20 and positivity for chromogranin A and synaptophysin (Table 1). None of the other tumors, including a MCPyV-positive BCC tumor, displayed the same staining pattern.

In our MCC series, none of the MCC patients were immunocompromised, except for Case 2 in which primary MCC had developed within 2 months after a living donor liver transplantation for fulminant hepatitis of unknown etiology. The patient passed away after 18 months because of MCC recurrence and metastasis. Cases 1, 4, 5, and 6 involved limited disease without metastasis or recurrence, while Cases 2, 3, 7, 8, and 9 involved synchronous or metachronous metastases.

PCR Amplification of MCPyV from Skin Tumors

We first analyzed whether MCPyV DNA fragments were present or absent in skin tumor tissues by conventional PCR. Nested PCR was performed in order to detect the 6 MCPyV DNA fragments using DNA samples extracted from tissue samples. The results are presented in Fig. 1 and Table 2. Positive results were obtained in all 9 MCC cases (100%), in 1 of 46 BCC cases (2.2%), and in 3 of 52 AK cases (5.8%). No PCR amplification fragments were observed in any of the other skin tumors, such as BD (n = 34), seborrheic keratosis (SK; n = 5), primary cutaneous anaplastic large-cell lymphoma (PCALCL; n = 5), malignant melanoma (MM; n = 5), or melanocytic nevus (MN; n = 6). Among the 6 fragments examined, the ST and LT1 fragments were amplified in 13 and 12 cases, respectively, while LT2 was the fragment that was most frequently absent from the tumors (it was only observed in 6 cases). As a result, all 6 fragments were amplified in 7 cases (4 of 9

Table 1. Clinicopathological data of Merkel cell polyomavirus (MCPyV)-positive skin tumors.

	Case	Age/ sex	Tumor size	Clinical course and follow up	Immunocompromised or not	Immunohistochemistry		
						CK20	Chromogranin A	Synaptophysin
MCC	1	71/F	2.1×2.0×1.8 cm	No recurrence or metastasis at 2 years	No	dot, 30%	weak, 100%	–
	2	62/M	3.5×2.5×2.5 cm	Primary tumor found after 2 months post living-donor liver transplantation. Lymph node metastasis at 6 months. Death at 18 months with MCC.	Yes	dot, 100%	weak, 100%	weak, 100%
	3	73/M	7.0×5.6×1.2 cm	Primary buttock MCC with multiple inguinal and pelvic lymph node metastases. Death at 6 months with MCC.	No	dot & cytoplasmic, 90%	100%	weak, 10%
	4	73/F	1.4×0.9×0.2 cm	No recurrence or metastasis at 14 months.	No	dot, 90%	60%	100%
	5	59/F	0.9 cm	No recurrence or metastasis at 70 months.	No	dot & cytoplasmic, 80%	100%	100%
	6	77/M	2.7×2.6×1.0 cm	No recurrence or metastasis at 22 months. Lost to follow up.	No	dot, 100%	100%	100%
	7	76/F	5.4×3.5 cm	Multiple liver metastases after 2 months. Death at 3 months	No	dot, 90%	50%	90%
	8	79/F	2.4×2.2×1.8 cm	Multiple skin metastases after 10 months. Systemic metastases at 12 months. Lost to follow up.	No	dot, 90%	10%	100%
	9	92/F	4.1×2.5×2.5 cm	Multiple lymph node metastases after 6 months. Lost to follow up.	No	dot, 60%	20%	100%
BCC	1	80/F	0.4×0.3 cm	No recurrence or metastasis.	No	–	–	–
AK	1	83/F	1.0×1.0 cm		No	–	–	–
	2	63/M	1.1×1.0 cm		No	–	–	–
	3	79/F	0.8×0.6 cm		No	–	–	–

MCC, Merkel cell carcinoma; BCC, Basal cell carcinoma; AK, Actinic keratosis; CK20, Cytokeratin20.

doi:10.1371/journal.pone.0039954.t001

MCC, 1 BCC, and 2 of 3 AK). In MCC, all 6 MCPyV fragments were detected in cases involving limited disease without distant metastases (Cases 1, 4, and 6), while 1 or more of the fragments was absent in 5 cases, 4 of which involved synchronous or metachronous metastases (Cases 2, 3, 7, and 8). The amplification pattern was the same in the primary and metastatic tumors in Cases 2 and 3, but an additional loss of amplification was observed in 1 of the 2 metastases in Case 8. PCR amplifications were unstable in AK cases 2 and 3 where we observed significant gel bands 2 to 4 times in 5 to 6 trials of the ST, VP1, and VP2 assays.

All PCR fragments in positive MCC, BCC, and AK cases were subjected to DNA sequencing and confirmed to belong to the MCPyV sequence. The full-length T-antigen sequence of MCPyV from the BCC case was not determined because of the small amount of available DNA.

Immunohistochemical Analysis of the MCPyV T Antigen in Skin Tumors

Immunohistochemical analyses of MCPyV were performed to determine the cellular localization and histological distribution of the virus in tumor tissues. Full-section skin-tumor slides were immunohistochemically analyzed with an antibody (CM2B4) against the MCPyV T antigen (Fig. 2). Most MCC cases (8/9) and 1 BCC case (1/46) were positive for the MCPyV T antigen, and they all were also found to be positive in the PCR analysis (Table 2). A diffuse nuclear staining pattern was observed in most of the positive cases. The labeling ratio ranged from 80% to 100%, except for in 1 case (Case 1, 30%). The staining intensity of the tumor cell nuclei was strong in 4 cases, including the BCC case, while it was diffusely weak and/or heterogeneous in the other cases. In contrast to the positive PCR results, no positive staining was observed in AK tumors. No immunoreactivity for the MCPyV T antigen was detected in BD (n = 34), SK (n = 5), PCALCL (n = 5), MM (n = 5), or MN (n = 6) tissues, and these results were consistent with the PCR results.

Copy Number of MCPyV in Skin Tumors

In order to further investigate the mode of infection and discrepancies between the PCR and immunohistochemistry results, we performed digital-PCR-based quantitation of the absolute viral copy number per human genome in MCPyV-infected tumor tissue. Digital PCR analyses were performed using a DNA template that was extracted from full-section slides. Case 4 was excluded from the digital PCR analysis because its tumor cell ratio was very low (approximately 3%). We designed a MCPyV-specific primer set that targeted the ST region because this fragment was amplified in all infected cases in the present study (Fig. 1 and Table 1). The ST region overlaps with the target regions of the LT3 primer sets that were used in previous studies [8,29,34]. In order to avoid possible assay errors due to MCPyV sequence diversity, we confirmed the digital PCR results with an additional second primer set and found that those results were reproducible (data not shown). As a human genome reference, we used the RNaseP gene, a single copy of which exists per human haploid genome [32,33]. We performed a dual-color assay and used the results to calculate the absolute viral copy number per haploid human genome (Fig. 3). In MCC, the tissue viral load varied from 0.119 to 42.843 (copies/haploid genome), but was mostly distributed around 1 (Fig. 3 and Table 2). The viral load was generally lower by 1 order of magnitude in AK tissue (between 0.019 and 0.068). The negative immunohistochemical results for 1 MCC and 3 AK cases were clearly linked to their low viral loads. The viral load of MCPyV-positive BCC was more similar to that of MCC tumors (0.662).

Methylation Status of Skin Tumors

The epigenetic silencing of tumor suppressor genes, such as the RASSF1A promoter, plays a characteristic and essential role in cancer development. Host RASSF1A DNA hypermethylation has been demonstrated in SV40 polyomavirus-related tumors and cell lines and in some cases of MCC [35,36]. Thus, our skin tumor samples were subjected to methylation-specific PCR analyses.

RASSF1A hypermethylation was detected in 6 of 9 MCC cases (67%), 7 of 46 BCC cases (15%), and 1 of 52 AK cases (1.9%) (Table 2). Interestingly, RASSF1A promoter hypermethylation was also observed in MCPyV-positive BCC. No promoter hypermethylation was seen in any other of the following skin tumors: PCALCL (n = 5), MM (n = 5), MN (n = 6), SK (n = 5), or

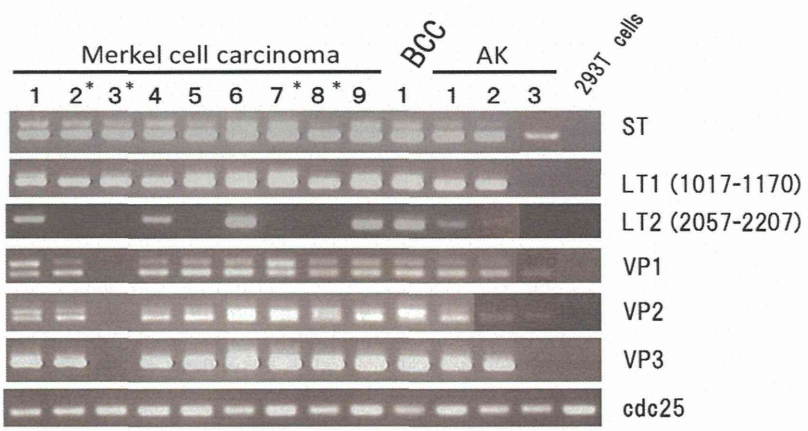

Figure 1. Polymerase chain reaction (PCR) amplification of the Merkel cell polyomavirus in the skin tumors. Six MCPyV gene fragments were detected in Merkel cell carcinoma, basal cell carcinoma (BCC), and actinic keratosis (AK). Cases involving synchronous or metachronous metastases are marked with an asterisk. Specific PCR fragments, including large T (LT)2, VP1, and VP2, were not amplified constantly in AK cases 2 and 3 (see text). To clarify, we replaced this part with a picture of successful amplification in another trial. Abbreviations: BCC, basal cell carcinoma; AK, actinic keratosis; 293T, polyomavirus SV40 T antigen-positive 293 cells. The lower panel indicates the single PCR proliferation band of the CDC25 gene.
doi:10.1371/journal.pone.0039954.g001

Table 2. Polymerase chain reaction, immunohistochemistry, and viral copy number per haploid human genome of MCPyV-positive skin tumors.

	Case		ST	LT1	LT2	VP1	VP2	VP3	IHC (MCPyV)	IHC staining pattern	viral CN per haploid human genome	Tumor ratio	RASSF1A hypermethylation
MCC	1	Tumor	+	+	+	+	+	+	+(30%)	heterogeneous partial	42.843	4	U
	2	Tumor	+	+	−	+	+	+	+(90%)	strong diffuse	0.369	4	M/U
		MLNM	+	+	−	+	+	+					
	3	Tumor	+	+	−	−	−	−	+(90%)	weak diffuse	1.361	4	M/U
		MLNM	+	+	−	−	−	−					
	4	Tumor	+	+	+	+	+	+	+(100%)	heterogeneous diffuse		1	M/U
	5	Tumor	+	+	−	+	+	+	−	−	0.119	2	M/U
	6	Tumor	+	+	+	+	+	+	+(80%)	heterogeneous diffuse	1.253	4	U
	7	Tumor	+	+	−	+	+	+	+(90%)	heterogeneous diffuse	1.065	4	U
	8	Tumor	+	+	−	+	+	+	+(100%)	strong diffuse	0.759	4	M/U
		Skin metastasis	+	+	−	+	+	+					
		Skin metastasis	+	+	−	−	−	+					
	9	Tumor	+	+	+	+	+	+	+(100%)	strong diffuse	0.756	4	M/U
BCC	1	Tumor	+	+	+	+	+	+	+(100%)	strong diffuse	0.662	2	M/U
AK	1	Tumor	+	+	+	+	+	+	−	−	0.068	2	U
	2	Tumor	+	+	+	+	+	+	−	−	0.031	2	U
	3	Tumor	+	−	−	+	+	−	−	−	0.019	2	U

IHC, immunohistochemistry; MCC, Merkel cell carcinoma; BCC, Basal cell carcinoma; AK, Actinic keratosis; MLNM, Multiple lymph node metastases; ST, small T; LT, large T; CN, copy number, Tumor ratio: 1, <10%; 2, >10% and <30%; 3, >30% and <70%; 4, >70%.

doi:10.1371/journal.pone.0039954.t002

BD (n = 34). No promoter hypermethylation of FHIT or CDKN2A was identified in MCC, BCC, AK, or other skin tumors (data not shown).

Discussion

In the present study, the frequency of MCPyV infection in various skin tumors was analyzed by conventional PCR and immunohistochemistry, and digital PCR technology was applied to calculate the absolute viral copy number per haploid genome in these tumor tissues.

The 100% PCR-based MCPyV detection rate that was observed in MCC in this study was compatible with the findings of studies performed in the US and Europe, but it was somewhat higher than those reported in Australia and Japan [2–5,9,18,24]. The MCPyV detection rates in 2 reports from Europe [10] and Asia [26] were over 90%, and this was similar to our detection rate. One of the reasons for our 100% positive PCR results may be due to a simple sampling problem because of the limited number of cases, and another possible reason was MCPyV sequence polymorphism within primer design regions. In the present study, the nested primer sets targeting 6 different regions of MCPyV were adopted for viral detection [24]. Interestingly, loss of the LT2 fragment was frequently observed in metastatic MCC and in primary MCC that produced metastases. While all 6 MCPyV fragments were amplified in 3 of the 4 cases involving limited disease, the LT2 fragment was absent from 4 of the 5 cases involving synchronous or metachronous metastases. While it could be due to sequence diversity in these regions, it is possible that extensive somatic mutations or deletions in these regions could be associated with tumor progression. A previous study found that a mutation in the LT region produced oncogenic effects through a prematurely truncated LT protein [30,37]. Similar events have been demonstrated to be involved in the transformation process in animal polyomavirus models [38–41].

The presence and pathogenesis of MCPyV DNA in skin tumors other than MCC are controversial. In previous studies, MCPyV DNA was amplified by PCR from 32% of sporadic non-melanoma skin cancers, including BCC (36/96, 37.5% and 3/24, 12.5%), SCC (7/28, 25%), and BD (4/23, 17.4%) [4,42]. In contrast, an immunohistochemical study did not detect any positive BCC or SCC cases [28]. The major problem with these previous studies was the lack of a method for quantitatively assessing viral infection. Conventional PCR can amplify very small amounts of viral DNA and provide us with the same positive results in spite of different viral loads, whereas the immunohistochemical method is dependent on the level of protein expression and it is difficult to reliably detect low levels of proteins. In the present study, we used digital PCR technology to calculate the absolute viral load per haploid human genome. The nanofluidic-based physical separation of each DNA template makes this technology highly robust, despite differences in the PCR efficiencies of different primers, such as RNaseP and MCPyV ST. Assessing the absolute viral load per haploid human genome is highly informative. First, the viral load differed markedly between MCC (0.37–42.8) and AK

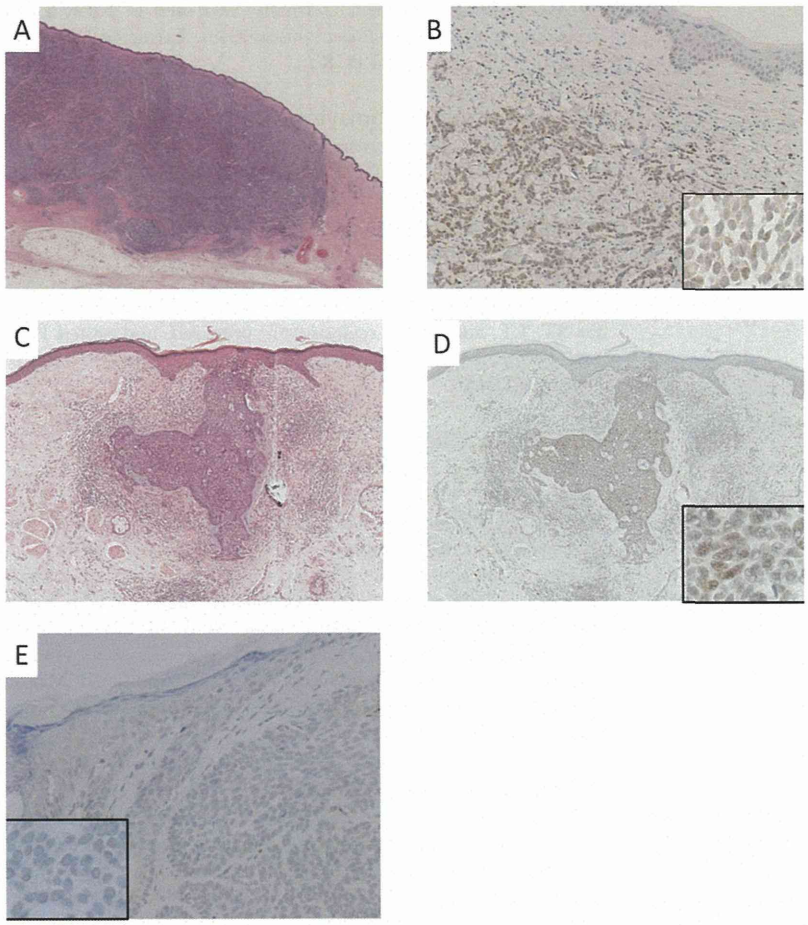

Figure 2. Morphology and immunohistochemical staining. Representative cases of Merkel cell carcinoma (MCC; A, B), a basal cell carcinoma (BCC)-positive case (C, D), and a BCC-negative case (E). Immunohistochemical staining with the anti-MCPyV large T-antigen antibody (CM2B4) (B, D, E). Heterogeneous and diffuse staining was observed in MCC (B), and strong diffuse positivity (D) and total negativity (E) was detected in BCC. Inset: Nuclear staining of MCPyV in MCC (B) and BCC (D,E).
doi:10.1371/journal.pone.0039954.g002

(0.02–0.07), suggesting that the biology of MCPyV infection differs between these 2 tumor groups. Second, there was a strong correlation between the immunohistochemical findings and viral load, which explains the conflicting results that were obtained with conventional PCR and immunohistochemistry. One possibility is that MCPyV-containing lymphocytes infiltrate within or around the atypical epidermis in AK. Another possibility is the infection of a small subset of tumor cells. It is worth noting that a lack of immunostaining and a relatively low copy number were observed in 1 MCC case (0.119 in Case 5). Therefore, we could not rule out the possibility that MCPyV had infected AK cells in our AK cases, and further studies are needed to examine this. Third, in most MCC cases, the MCPyV copy number per haploid genome was around 1. Taking the diffuse immunohistochemical staining seen in the majority of MCC cells into account, there is a realistic possibility that each MCC cell had clonally integrated 2 copies of the MCPyV genome, which could not be the case for AK.

In the present study, we observed the presence of MCPyV DNA fragments in 1 of 46 BCC cases (2.2%). The strong and diffusely positive immunohistochemical staining and moderate viral load (compared to that observed in the MCC) observed in this tumor confirmed that it had been infected by MCPyV. These findings suggest that MCPyV may also contribute to the development of the minority of sun-exposed skin tumors in addition to MCC. Interestingly, hypermethylation of RASSF1A was detected in this case of BCC, as was found in two-thirds of the MCC cases. Hypermethylation of host DNA has been detected in SV40 polyomavirus-related tumors and cell lines as well as in some MCC [13,14]. MCPyV infects progenitor skin endocrine cells, but it may sometimes infect cells that can differentiate into other cell types.

Although further studies are needed for a complete understanding of these results, our quantitative analysis of the viral load per haploid genome revealed that MCPyV infection displays different biological characteristics and epidemiology in skin tumor tissues.

Materials and Methods

Tissue and Cell Samples

Skin tumors, which were surgically resected or biopsied from 1996 to 2009, were retrieved from the database of the Department of Pathology, Tokyo University Hospital. Each histological diagnosis was independently confirmed by S.O and Y.T. Skin

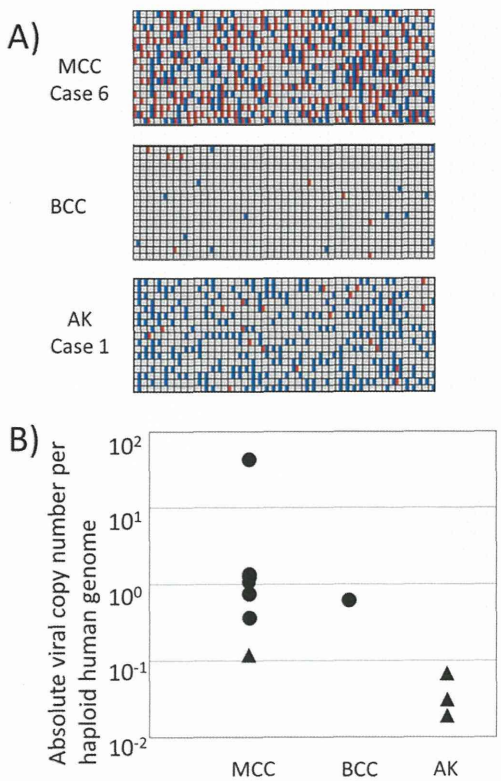

Figure 3. MCPyV copy number in various skin tumors. (A) Digital PCR software-generated composite heat maps showing chambers with positive signals for both control RNaseP genes (blue) and MCPyV (red). Digital PCR heat maps are indicated in the upper panel for Merkel cell carcinoma case 6, in the middle panel for basal cell carcinoma (positive case), and in the lower panel for actinic keratosis (case 1). (B) Scatter plot of the MCPyV copy number of Merkel cell carcinoma, basal cell carcinoma, and actinic keratosis. Immunohistochemically positive cases are shown as black dots (■), and negative cases are indicated by triangles (▲).
doi:10.1371/journal.pone.0039954.g003

tumors used in this study included MCC (n = 4), BCC (n = 46), AK (n = 52), BD (n = 34), SK (n = 5), PCALCL (n = 5), MM (n = 5), and MN (n = 6). Additionally, 5 cases of MCC from Toranomon Hospital were also analyzed. All of these tumors were fixed by formalin and embedded in paraffin for diagnostic purposes. Immunostaining of CK20, synaptophysin, and chromogranin A was used to confirm the diagnosis of MCC. This study was approved by the University of Tokyo Institutional Ethical Committee. Clinical samples with written informed consent were collected under the University of Tokyo Institutional guidelines for the study of human tissues.

As for the cultured cells, 293T cells (American Type Culture Collection, Manassas, VA) were maintained, as described previously.

Preparation of DNA from Paraffin-embedded Clinical Material

Serial sections of tumor specimens were subjected to hematoxylin and eosin staining, immunohistochemistry, and DNA preparation. To isolate DNA from formalin-fixed paraffin-embedded skin tumor samples, 3 10 μm-thick sections were placed into 1.5-mL sterile tubes, and a DNeasy Tissue Kit (QIAGEN GmbH, Hilden, Germany) was used to purify DNA according to the manufacturer's instructions. Extracted DNA was used for PCR and digital PCR.

PCR Primers for Polyomavirus DNA

The quality of DNA was checked by amplifying the cdc25 (forward: 5′-TGGTGGGCCAAACACTATCC-3′, reverse: 5′-ATCGTTGGGCTCGCAGATCACC-3′) and glyceraldehyde-3-phosphate dehydrogenase (forward: 5′-GAAGGTGAAGGTCG-GAGTC-3′, reverse: 5′-GAAGATGGTGATGGGATTC-3′) genes.

For MCPyV detection, 6 nested primer sets, including primers for ST, LT, and VP1-3 regions were prepared, and nested PCR was performed, as described previously [24], with 40 ng of extracted DNA.

DNA Sequencing

PCR-amplified fragments of MCPyV and other polyomaviruses were purified using MicroSpin S-300 HR Columns (GE Healthcare, Piscataway, NJ), and purified PCR products were then applied to an ABI sequencer (Life Technologies Corporation, Carlsbad, CA) and analyzed according to the manufacturer's protocol. All sequences of PCR-amplified fragments were compared to each other for similarity using NCBI-BLAST and were fully matched with the Merkel cell polyomavirus genome sequence, which was already reported [37]. Additional Merkel Cell Polyomavirus sequencing for hot spot in Large T antigen was analyzed in Figure S2.

Antibodies and Immunohistochemistry

Immunohistochemistry was applied to formalin-fixed and paraffin-embedded tissue samples in all cases. Immunohistochemistry was performed with monoclonal antibodies against the MCPyV LT antigen (CM2B4; Santa Cruz Biotechnology, Inc, Santa Cruz, CA, 1:50 dilution), CK20 (Leica Microsystems Inc, Buffalo Grove, IL, 1:100 dilution), chromogranin A (Dako Denmark A/S, Glostrup, Denmark, 1:200 dilution), and synaptophysin (Dako Denmark A/S, 1:100 dilution). Immunohistochemistry was performed according to standard techniques on a Ventana Benchmarks XT Autostainer (Ventana Medical Systems, Inc, Tucson, AZ) with the labeled streptavidin-biotin peroxidase method and diaminobenzidine visualization. Appropriate positive and negative controls were included for each immunohistochemical experiment.

Nuclear staining was considered to indicate positivity for the LT antigen of MCPyV.

Copy Number Assessment Using Digital PCR

A primer set targeting the ST region, which overlaps with the target regions of the LT3 primer sets used in previous studies, was designed (STF 576: 5′-TCGCCAGCATTGTAGTCTAAAAAC-3′; STR 668: 5′-CCAAACCAAAGAATAAAGCACTGA-3′, and ST probe: 5′-AGCAAAAACACTCTCCCCACGTCAGACA-3′) (Fig. S1). For additional digital PCR quantification, a second primer set was designed (STF 550: 5′-TGCGCTTGTAT-TAGCTGTAAGTTGT-3′; STR 640: 5′-AAAACACTCTCCC-CACGTCAGA-3′; and ST probe: 5′-AGCAAAAA-CACTCTCCCCACGTCAGACA-3′).

For each panel, 10 μL of reaction mixture containing 1 × TaqMan Gene Expression Master Mix (Life Technologies), 1 × RNase P-VIC TaqMan assay, 1 × MCPyV ST-FAM TaqMan assay (900 nM primers and 200 nM probe), 1 × sample loading reagent (Fluidigm Corporation, South San Francisco, CA), and

3.5 μL of extracted genomic DNA was prepared. The reaction mix was applied to the 12.765 digital array, which contained 765 small chambers for each sample, and was analyzed using the EP-1 system (Fluidigm Corporation) [33]. Thermocycling conditions included an initial step of 95°C for 10 min, which was followed by 40 cycles of 2-step PCR: 15 s at 95°C for denaturing and 1 min at 60°C for annealing and extension. Data was transformed from the observed positive chamber count to the estimated copy number using the mathematical formula described by Dube S et al. [32], and the absolute viral copy number per haploid genome was defined as the ratio of MCPyV ST copy number to RNaseP copy number. Tumor cell ratios were counted and graded as follows: 1, <10%; 2, >10% and <30%; 3, >30% and <70%; or 4, >70%. The absolute viral copy number per haploid genome by the second primer showed similar results (data not shown).

Methylation-specific PCR (MS-PCR)

Methylation analysis was performed to evaluate the promoter hypermethylation status of MCC, BCC, and AK. The promoter regions of RASSF1A, CDKN2A, and FHIT were examined, as described previously [10]. The extracted template DNA was modified by the bisulfite reaction using an EpiTect Bisulfite kit (QIAGEN GmbH). Methylation status was distinguished by MS-PCR using sequence-specific primer pairs. MS-PCR experiments were performed at least twice. PCR primers and conditions were described previously [10].

Supporting Information

Figure S1 The primer used for digital PCR targeting the ST region, which overlaps with the target regions of the LT3 primer that was previously reported by Feng.
(DOCX)

Figure S2 Merkel Cell Polyomavirus sequencing for hot spot in Large T antigen.
(DOC)

Acknowledgments

We would like to thank Aiko Nishimoto, Kei Sakuma, and Harumi Yamamura for their technical assistance.

Author Contributions

Conceived and designed the experiments: SO SI MF. Performed the experiments: SO SI YT AG TF KO. Analyzed the data: SO SI. Contributed reagents/materials/analysis tools: SO SI. Wrote the paper: SO.

References

1. LeBoit PE, Burg G, Weedon D, Sarasin A (2006) World Health Organization Classification of Tumours Pathology and Genetics Skin Tumours. IARC Press
2. Feng H, Shuda M, Chang Y, Moore PS (2008). Clonal integration of a polyomavirus in human Merkel cell carcinoma. Science 319: 1096–1100
3. Kassem A, Schopflin A, Diaz C, Weyers W, Stickeler E, et al. (2008) Frequent detection of Merkel cell polyomavirus in human Merkel cell carcinomas and identification of a unique deletion in the VP1 gene. Cancer Res. 68: 5009–5013
4. Becker JC, Houben R, Ugurel S, Trefzer U, Pfohler C, et al. (2009) MC polyomavirus is frequently present in Merkel cell carcinoma of European patients. J. Invest. Dermatol. 129: 248–250
5. Garneski KM, Warcola AH, Feng Q, Kiviat NB, Leonard JH, et al. (2009). Merkel cell polyomavirus is more frequently present in North American than Australian Merkel cell carcinoma tumors. J. Invest. Dermatol. 129: 246–248
6. Busam KJ, Jungbluth AA, Rekthman N, Coit D, Pulitzer M, et al. (2009) Merkel cell polyomavirus expression in Markel cell carcinomas and its absence in combined tumors and pulmonary neuroendocrine carcinomas. Am. J. Surg. Pathol. 33: 1378–1385
7. Ridd K, Yu S, Bastian BC (2009) The presence of polyomavirus in nonmelanoma skin cancer in organ transplant recipients is rare. J. Invest. Dermatol.129: 250–252.
8. Loyo M, Guerrero-Preston R, Brait M, Hoque MO, Chuang A, et al. (2010) Quantitative detection of Merkel cell virus in human tissues and possible mode of transmission. Int. J. Cancer 126: 2991–2996
9. Foulongne V, Dereure O, Kluger N, Moles JP, Guillot B, et al. (2010) Merkel cell polyomavirus DNA detection in lesional and nonlesional skin from patients with Merkel cell carcinoma or other skin diseases. Br. J. Dermatol. 162: 59–63
10. Helmbold P, Lahtz C, Enk A, Herrmann-Trost P, Marsch WCh, et al. (2009) Frequent occurrence of RASSF1A promoter hypermethylation and Merkel cell polyomavirus in Merkel cell carcinoma. Mol. Carcinog. 48: 903–909
11. Paulson KG, Lemos BD, Feng B, Jaimes N, Peñas PF, et al. (2009) Array-CGH reveals recurrent genomic changes in Merkel cell carcinoma including amplification of L-Myc. J. Invest. Dermatol. 129: 1547–1555.
12. Duncavage EJ, Zehnbauer BA, Pfeifer JD (2009) Prevalence of Merkel cell polyomavirus in Merkel cell carcinoma. Mod. Pathol. 22: 516–521.
13. Bhatia K, Goedert JJ, Modali R, Preiss L, Ayers LW (2010) Merkel cell carcinoma subgroups by Merkel cell polyomavirus DNA relative abundance and oncogene expression. Int. J. Cancer 126: 2240–2246.
14. Carter JJ, Paulson KG, Wipf GC, Miranda D, Madeleine MM, et al. (2009) Association of Merkel cell polyomavirus–specific antibodies with Merkel cell carcinoma. J. Natl. Cancer Inst. 101: 1510–1522.
15. Andres C, Belloni B, Puchta U, Sander CA, Flaig MJ (2010) Prevalence of MCPyV in Merkel cell carcinoma and non-MCC tumors. J. Cutan. Pathol. 37: 28–34
16. Houben R, Schrama D, Alb M, Pföhler C, Trefzer U, et al. (2010) Comparable expression and phosphorylation of the retinoblastoma protein in Merkel cell polyoma virus–positive and negative Merkel cell carcinoma. Int. J. Cancer 126: 796–798.
17. Wieland U, Mauch C, Kreuter A, Krieg T, Pfister H (2009) Merkel cell polyomavirus DNA in persons without Merkel cell carcinoma. Emerg. Infect. Dis. 15: 1496–1498.
18. Sastre-Garau X, Peter M, Avril MF, Laude H, Couturier J, et al. (2009) Merkel cell carcinoma of the skin: pathological and molecular evidence for a causative role of MCV in oncogenesis. J. Pathol. 218: 48–56.
19. Touzé A, Gaitan J, Maruani A, Le Bidre E, Doussinaud A, et al. (2009) Merkel cell polyomavirus strains in patients with Merkel cell carcinoma. Emerg. Infect. Dis. 15: 960–962.
20. Wetzels CT, Hoefnagel JG, Bakkers JM, Dijkman HB, Blokx WA, et al. (2009) Ultrastructural proof of polyomavirus in Merkel cell carcinoma tumour cells and its absence in small cell carcinoma of the lung. PLoS ONE 4: e4958.
21. Sihto H, Kukko H, Koljonen V, Sankila R, Böhling T, et al. (2009) Clinical factors associated with Merkel cell polyomavirus infection in Merkel cell carcinoma. J. Natl. Cancer Inst. 101: 938–945.
22. Varga E, Kiss M, Szabó K, Kemény L (2009) Detection of Merkel cell polyomavirus DNA in Merkel cell carcinomas. Br. J. Dermatol. 161: 930–2.
23. Mangana J, Dziunycz P, Kerl K, Dummer R, Cozzio A (2010) Prevalence of Merkel cell polyomavirus among Swiss Merkel cell carcinoma patients. Dermatology 221: 184–188
24. Katano H, Ito H, Suzuki Y, Nakamura T, Sato Y, et al. (2009) Detection of Merkel cell polyomavirus in Merkel cell carcinoma and Kaposi's sarcoma. J. Med. Virol. 81: 1951–1958
25. Nakajima H, Takaishi M, Yamamoto M, Kamijima R, Kodama H, et al. (2009) Screening of the specific polyoma virus as diagnostic and prognostic tools for Merkel cell carcinoma. J. Dermatol. Sci. 56: 211–213.
26. Woo KJ, Choi YL, Jung HS, Jung G, Shin YK, et al. (2010) Merkel cell carcinoma: our experience with seven patients in Korea and a literature review. J. Plast. Reconstr. Aesthet. Surg. 63: 2064–2070.
27. Kuwamoto S, Higaki H, Kanai K, Iwasaki T, Sano H, et al. (2011) Association of Merkel cell polyomavirus infection with morphologic differences in Merkel cell carcinoma. Human Pathol. 42: 632–640.
28. Reisinger DM, Shiffer JD, Cognetta AB Jr, Chang Y, Moore PS (2010) Lack of evidence for basal or squamous cell carcinoma infection with Merkel cell polyomavirus in immunocompetent patients with Merkel cell carcinoma. J. Am. Acad. Dermatol. 63: 400–403
29. Shuda M, Arora R, Kwun HJ, Feng H, Sarid R, et al. (2009) Human Merkel cell polyomavirus infection I. MCV T antigen expression in Merkel cell carcinoma, lymphoid tissues and lymphoid tumors. Int. J. Cancer 125: 1243–1249
30. Shuda M, Kwun HJ, Feng H, Chang Y, Moore PS (2011) Human Merkel cell polyomavirus small T antigen is an oncoprotein targeting the 4E-BP1 translation regulator. J. Clin. Invest. 121: 3623–3634
31. Neumann F, Borchert S, Schmidt C, Reimer R, Hohenberg H, et al. (2011) Replication, gene expression and particle production by a consensus Merkel Cell Polyomavirus (MCPyV) genome. PLoS One 6: e29112
32. Dube S, Qin J, Ramakrishnan R (2008) Mathematical analysis of copy number variation in a DNA sample using digital PCR on a nanofluidic device. PLoS. One 3: e2876

33. Qin J, Jones RC, Ramakrishnan R (2008) Studying copy number variations using a nanofluidic platform. Nucleic Acids Res. 36: e116
34. Fischer N, Brandner J, Fuchs F, Moll I, Grundhoff A (2010) Detection of Merkel cell polyomavirus (MCPyV) in Merkel cell carcinoma cell lines: cell morphology and growth phenotype do not reflect presence of the virus. Int. J. Cancer 126: 2133–2142
35. Toyooka S, Pass HI, Shivapurkar N, Fukuyama Y, Maruyama R, et al. (2001) Aberrant methylation and simian virus 40 tag sequences in malignant mesothelioma. Cancer Res. 61: 5727–5730
36. Toyooka S, Carbone M, Toyooka KO, Bocchetta M, Shivapurkar N, et al. (2002) Progressive aberrant methylation of the RASSF1A gene in simian virus 40 infected human mesothelial cells. Oncogene 21: 4340–4344
37. Shuda M, Feng H, Kwun HJ, Rosen ST, Gjoerup O, et al. (2008) T antigen mutations are a human tumor-specific signature for Merkel cell polyomavirus. Proc. Natl. Acad. Sci. U S A 105: 16272–16277
38. Small MB, Gluzman Y, Ozer HL (1982) Enhanced transformation of human fibroblasts by origin-defective simian virus 40. Nature 296: 671–672
39. Prives C, Covey L, Scheller A, Gluzman Y (1983) DNA-binding properties of simian virus 40 T-antigen mutants defective in viral DNA replication. Mol. Cell. Biol. 3: 1958–1966
40. Manos MM, Gluzman Y (1984) Simian virus 40 large T-antigen point mutants that are defective in viral DNA replication but competent in oncogenic transformation. Mol. Cell. Biol. 4: 1125–1133
41. Lania L, Hayday A, Fried M (1981) Loss of functional large T-antigen and free viral genomes from cells transformed in vitro by polyoma virus after passage in vivo as tumor cells. J. Virol. 39: 422–431
42. Kassem A, Technau K, Kurz AK, Pantulu D, Loning M, et al. (2009) Merkel cell polyomavirus sequences are frequently detected in nonmelanoma skin cancer of immunosuppressed patients. Int. J. Cancer 125: 356–361

OPEN ACCESS Freely available online

PLOS ONE

Macrophages, Nitric Oxide and microRNAs Are Associated with DNA Damage Response Pathway and Senescence in Inflammatory Bowel Disease

Jane J. Sohn[1], Aaron J. Schetter[1☯], Harris G. Yfantis[2☯], Lisa A. Ridnour[3], Izumi Horikawa[1], Mohammed A. Khan[1], Ana I. Robles[1], S. Perwez Hussain[1], Akiteru Goto[1], Elise D. Bowman[1], Lorne J. Hofseth[4], Jirina Bartkova[5], Jiri Bartek[5,6], Gerald N. Wogan[7], David A. Wink[3], Curtis C. Harris[1]*

1 Laboratory of Human Carcinogenesis, Center for Cancer Research, National Cancer Institute, Bethesda, Maryland, United States of America, **2** Pathology and Laboratory Medicine, Baltimore Veterans Affairs Medical Center, and Department of Pathology, University of Maryland School of Medicine, Baltimore, Maryland, United States of America, **3** Radiation Biology Branch, National Cancer Institute, Bethesda, Maryland, United States of America, **4** Department of Pharmaceutical and Biomedical Sciences, South Carolina College of Pharmacy, University of South Carolina, Columbia, South Carolina, United States of America, **5** Cancer Society Research Center, Copenhagen, Denmark, **6** Institute of Molecular and Translational Medicine, Faculty of Medicine and Dentistry, Palacky University, Olomouc, Czech Republic, **7** Department of Biological Engineering, Center for Environmental Health Sciences, Massachusetts Institute of Technology, Cambridge, Massachusetts, United States of America

Abstract

Background: Cellular senescence can be a functional barrier to carcinogenesis. We hypothesized that inflammation modulates carcinogenesis through senescence and DNA damage response (DDR). We examined the association between senescence and DDR with macrophage levels in inflammatory bowel disease (IBD). *In vitro* experiments tested the ability of macrophages to induce senescence in primary cells. Inflammation modulating microRNAs were identified in senescence colon tissue for further investigation.

Methodology/Principal Findings: Quantitative immunohistochemistry identified protein expression by colon cell type. Increased cellular senescence (HP1γ; $P = 0.01$) or DDR (γH2A.X; $P = 0.031$, phospho-Chk2, $P = 0.014$) was associated with high macrophage infiltration in UC. Co-culture with macrophages (ANA-1) induced senescence in >80% of primary cells (fibroblasts MRC5, WI38), illustrating that macrophages induce senescence. Interestingly, macrophage-induced senescence was partly dependent on nitric oxide synthase, and clinically relevant NO• levels alone induced senescence. NO• induced DDR *in vitro*, as detected by immunofluorescence. In contrast to UC, we noted in Crohn's disease (CD) that senescence (HP1γ; $P<0.001$) and DDR (γH2A.X; $P<0.05$, phospho-Chk2; $P<0.001$) were higher, and macrophages were not associated with senescence. We hypothesize that nitric oxide may modulate senescence in CD; epithelial cells of CD had higher levels of NOS2 expression than in UC ($P = 0.001$). Microarrays and quantitative-PCR identified miR-21 expression associated with macrophage infiltration and NOS2 expression.

Conclusions: Senescence was observed in IBD with senescence-associated β-galactosidase and HP1γ. Macrophages were associated with senescence and DDR in UC, and *in vitro* experiments with primary human cells showed that macrophages induce senescence, partly through NO•, and that NO• can induce DDR associated with senescence. Future experiments will investigate the role of NO• and miR-21 in senescence. This is the first study to implicate macrophages and nitrosative stress in a direct effect on senescence and DDR, which is relevant to many diseases of inflammation, cancer, and aging.

Citation: Sohn JJ, Schetter AJ, Yfantis HG, Ridnour LA, Horikawa I, et al. (2012) Macrophages, Nitric Oxide and microRNAs Are Associated with DNA Damage Response Pathway and Senescence in Inflammatory Bowel Disease. PLoS ONE 7(9): e44156. doi:10.1371/journal.pone.0044156

Editor: Benoit Foligne, Institut Pasteur de Lille, France

Received April 10, 2012; **Accepted** July 30, 2012; **Published** September 6, 2012

Funding: This research was supported by the Intramural Research Program of the National Cancer Institute. Dr. Sohn was supported by the Cancer Research Training Award Fellowship from the National Cancer Institute. Dr. Bartkova and Dr. Bartek were supported by the Danish Cancer Society, the Danish National Research Foundation, and the European Commission (projects: Infla-Care, Biomedreg and DDResponse). The funders had no role in study design, data collection and analysis, decision to publish, or preparation of the manuscript.

Competing Interests: The authors have declared that no competing interests exist.

* E-mail: Curtis_Harris@nih.gov

☯ These authors contributed equally to this work.

Introduction

Inflammatory bowel disease (IBD) is associated with high morbidity, poor quality of life and an increased risk of colon cancer in over 3.5 million people in the United States and Europe, with a steadily growing prevalence in Asia [1]. The most important risk factors for colon cancer development in IBD patients are duration and extent of inflammation. Patients with ulcerative colitis (UC), a subtype of IBD, develop colon cancer with a five-fold overall relative risk compared to population controls [2]. Colon tissue from IBD patients has been used to study the relationship between inflammation and cancer, with an emphasis on DNA damage. IBD is associated

with increased etheno-DNA adducts [3], microsatellite instability [4], p53 mutational load [5] and clonal expansion of cells with mutations in polyguanine tracts [6]. UC tissues show initial activation of p53 in response to nitric oxide (NO•) [7], and eventual inactivation of p53 with increasing mutation load [5], resulting in a pattern of mutation unique compared to spontaneous colon cancer [8].

Evidence suggests that senescence acts as a barrier to carcinogenesis in UC and that this barrier is reduced in dysplastic lesions [9]. Inflamed colons from UC patients have increased expression of the DNA damage response pathway (DDR) sensor protein γH2A.X [10], which leads to activation of the stress-associated p53 pathway. DDR is implicated in the induction of premature cellular senescence [11,12], independently of telomere length, which classically regulates senescence [13] in cellular aging. Prosenescent cytokines [14], WNT16 [15], and the Rb/p16 [16] pathway (through its induction of heterochromatin formation with HP1γ positive foci [17]), have all been implicated in premature cellular senescence. Premature cellular senescence halts carcinogenesis by limiting the proliferation of cells in the early stages of carcinogenesis [12,18–20]. Senescence during inflammation is not well studied, but experiments *in vitro* have shown increased p53 and p21, in response to oxidative stress induced senescence [21,22]. Elucidating the cause and outcome of inflammation-associated senescence is relevant for the 25% of human cancers associated with chronic inflammation and infection [23,24].

Macrophages are a key component of a chronic inflammatory response and constitute part of the heterogeneous population of cells in tumors. Macrophages and NO• has been implicated in the activation of p53 [7] in IBD and the activation of the Akt pathway in breast cancer [25]. In addition, tumor-associated macrophages are implicated in carcinogenesis [26,27]. We hypothesized that macrophages accelerate cellular senescence in epithelial cells at risk for carcinogenesis through the DNA damage pathway, in a NO• -dependent manner. NO• secreted by macrophages rapidly decreases in concentration with diffusion [28], thus cells may be exposed to different levels of NO• depending on distance from an NO• producing macrophage [29]. Stromal fibroblasts can be cellular targets of NO• and become senescent and secrete pro-inflammatory cytokines such as IL-6 and IL-8 [30]. We quantified macrophages in the lamina propria using quantitative immunohistochemistry (IHC) to identify macrophage numbers within the mucosa (i.e. macrophage infiltration). Levels of macrophage infiltration were correlated to DDR and senescence. Normal colonic epithelial cells can produce endogenous NO•, thus we also measured levels of NOS2 by IHC in the epithelium. Further, we determined if macrophages and NO• induce cellular senescence *in vitro*.

MicroRNAs (miRs) have been shown to be involved in nearly every biological process examined, including inflammation and senescence. To investigate the potential for miRs to be involved in macrophage or NOS2- induced senescence, we also evaluated the association of microRNAs with macrophage infiltration and NOS2 in IBD, and colonic adenomas.

Methods and Patients

Ethics Statement

This study was approved by the Institutional Review Board of the National Cancer Institute (OHSRP 3637, OHSRP 3961).

Tissues

Colon tissues from UC and CD patients and colon adenomas were obtained from the Cooperative Human Tissue Network (Philadelphia, PA; Table S1). Two samples with varying degrees of gross inflammation were taken from each patient. Normal colons were obtained from University of Maryland, with tissues collected within 2 hours of death from patients who died of traumatic causes, were donors for organ transplants, and had no diseases related to the colon or chronic inflammation (Department of Pathology, University of Maryland, Baltimore, MD). Consent for the use of the tissues for research purposes was provided by next of kin or legally responsible individual on behalf of the deceased prior to the autopsy being performed. Investigators were not provided with any personal identifiers for these tissues and all patients were anonymous. Detailed clinical history was not provided, and the information on the extent of disease involvement in the small and large bowels was limited.

Tissues for IHC were fixed in 10% neutral buffered formalin, and embedded in paraffin. Samples without epithelial cells were excluded. A total of 29 UC colons, and 32 CD colons, and 5 normal colons met these criteria.

Immunohistochemical Analysis

Immunohistochemistry (IHC) for DDR markers γH2A.X, phospho-Chk2, p53, and $p21^{WAF1}$ was quantified by counting the number of positive epithelial cells versus total epithelial cells in three 250× magnification fields. An average of 3214 (UC) and 3178 epithelial cells (CD) were counted per sample in a blinded fashion by H. Y, a board certified pathologist. IHC for the monocyte and macrophage marker, CD68, was quantified by counting the number of stromal cells in the lamina propria. IHC for NOS2 was quantified by counting the number of epithelial and stromal cells in the lamina propria. Percent positivity was calculated by dividing the number of positive cells over total cells for each enumerated marker. For HP1γ, a combined score of intensity and distribution was used to score staining on a scale of 1–4 [31] to reflect the marked differences in both intensity and number of positive cells between UC and CD. All antibodies and further details are available in Materials and Methods S1. Antibodies for total Chk2 were tested by immunoblot for specificity (Figure S1) as described in the Materials and Methods S1.

Coculture and Cell Culture Treatment

Normal human fibroblast strains MRC-5 and WI-38 (Coriell Institute for Medical Research, Camden, NJ), and murine macrophage strain ANA-1 [32] were grown in phenol red-free DMEM supplemented with 10% FBS (Biofluids, Rockville, MD), 4 mM glutamine (Biofluids), penicillin (10 units/ml), and streptomycin (10 μg/ml, Biofluids).

Cocultures were established by seeding 2500 normal human fibroblasts and 833 macrophages per well (3:1 ratio) in a 6-well dish with 2 mL of media and cultured for 7 days. 200 μL of media was removed and replaced each day to replenish media contents. Fibroblasts were exposed to spermine NONOate (Sper/NO•; Sigma-Aldrich, St. Louis) as a NO• donor, or hydrogen peroxide (control) overnight (16 hrs) to evaluate induction of senescence in normal human fibroblasts. All experiments were repeated three times with three technical replicates for each repetition. At least 1500 cells were evaluated for senescence in each repetition using senescence-associated β-galactosidase (SA β-gal) buffer at pH 6.0 [33]. See Materials and Methods S1 for further details.

Results

UC and CD have Increased Macrophage Infiltration Compared to Normal Tissues

Both UC and CD had increased densities of macrophages, indicated by CD68+ cells, when compared to normal colons ($P<0.05$; Figure S2), reflective of the increased inflammation expected in UC and CD. UC and CD colons showed similar numbers of macrophages ($P>0.05$) compared to each other. The number of CD68+ cells was used to stratify tissues for this study; colons with macrophage numbers above the median were defined as having "high macrophage index".

Macrophage Infiltration is Positively Associated with Cellular Senescence in UC

We measured HP1γ as an indicator of cellular senescence in formalin-fixed paraffin-embedded (FFPE) tissue. HP1γ localizes to senescence-associated heterochromatin foci *in vitro* [17], and correlates to SAβ-gal [33] in fresh colonic adenomas [12]. High macrophage index was associated with elevated staining for HP1γ in colonic epithelial cells of UC patients ($P=0.01$). Macrophages in UC correlated with HP1γ in epithelial cells ($P=0.025$; *Spearman* $=0.43$), indicating that macrophage infiltration is associated with senescence in nearby epithelial cells. In contrast, CD colonic epithelial cells had higher levels of HP1γ than UC ($P<0.001$; Figure 1A). HP1γ was not associated with high macrophage index in CD patients (Figure 1A), suggesting there may be other factors contributing to senescence in CD versus UC. Examples of strong HP1γ in CD, moderate staining in UC, and negative staining in normal tissues is shown (Figure 1B–D). Strong staining in colon adenoma (positive control) is shown in Figure S3E.

We next examined senescence-associated β-galactosidase (SAβ-gal) activity in frozen sections of UC and CD patients to confirm the presence of cellular senescence because enzyme activity is considered the gold standard. Fresh tissue is optimal for testing enzyme activity, but only archival frozen tissue was available for this study. Long-term storage of archival tissue may degrade enzyme activity, leading to false negatives, yet we were able to detect SAβ-gal activity in 13/21 (62%) UC and in 14/38 (37%) CD colons, illustrating for the first time that SAβ-gal-associated senescence is present in IBD tissue (Figure S3A-D). Immortalized normal human fibroblasts treated with Nutlin-3A [34] were used as positive controls.

Activation of DDR (γ-H2A.X and Phospho-Chk2) is Higher in CD and UC than in Normal Tissue

We determined levels of DDR markers associated with premature senescence [11,12] by IHC in the epithelial cells of IBD and normal colons. UC and CD colons showed increased levels of γH2A.X ($P<0.05$; $P<0.001$), phospho-Chk2 ($P<0.01$, $P<0.001$), p53 ($P<0.01$), and p21 ($P<0.05$) when compared to normal colons (Figure 2A). No increase was observed in total Chk2 in IBD versus normal colons, consistent with previous data that Chk2 is unchanged during colon carcinogenesis [11].

We found that UC colons had lower levels of DDR compared to CD, based on γH2A.X ($P<0.05$) and phospho-Chk2 ($P<0.001$) staining. No differences were observed in total Chk2, p53 or p21 between CD and UC (Figure 2A). Examples of staining patterns are shown in Figure S4.

Macrophages are Positively Associated with Activation of DDR in UC

We examined if high macrophage index was associated with activation of DDR. In UC patients, high macrophage index was associated with increased γH2A.X ($P=0.031$) and phospho-Chk2 ($P=0.014$; Figure 2B) in colonic epithelium. No significant differences were observed for p53, or p21, although p21 was marginally increased in tissues with higher macrophage index (Figure 2B). In colons from CD patients, macrophage index was not associated with either activation of the DDR pathway or immunopositivity of p21 (Figure S5).

We hypothesized that macrophages directly induce senescence, based on the data from UC tissues. To test this, we performed the following *in vitro* experiments with macrophages and primary human cells.

Macrophages cause NO• Induced Cellular Senescence *in vitro*

To investigate the role of macrophages in the induction of senescence *in vitro*, normal, primary human fibroblast strains MRC5 and WI38 were cocultured with macrophages for 7 days and evaluated by the SA-βgal assay. Fibroblasts are relevant because senescent stromal cells can produce proinflammatory cytokines that may influence the senescent state of epithelial cells. Approximately eighty percent of fibroblasts cocultured with macrophages were positive for SA-βgal, and showed more senescent blue-stained cells compared to fibroblasts grown alone (Figure 3A; WI38, $P=0.002$; MRC5, $P=0.003$).

To determine if NO• produced by macrophages may be capable of inducing senescence in stromal fibroblasts, macrophages and fibroblasts were cocultured in media with and without the NO• synthase inhibitor *N*-nitro-l-arginine methyl ester (L-NAME, 500 μM, Sigma-Aldrich, St. Louis). DAF-FM diacetate (4-amino-5-methylamino-2′, 7′-difluorofluorescein diacetate; DAF, Invitrogen, Carlsbad) was used to assess the amount of NO• diffused into the media of cocultured cells. As expected, L-NAME led to decreased NO• present in the media of cocultures (Figure 3B; WI38, $P=0.008$, MRC5; $P=0.03$). After exposure to coculture, fibroblasts were fixed and stained for SA-βgal activity at pH 6.0, resulting in blue substrate in senescent cells (Figure S6.) Cocultures grown in the presence of L-NAME showed decreased blue SA-βgal positive cells (Figure 3A; WI38, $P=0.002$; MRC5, $P=0.003$). This suggested that NO• is at least partially responsible for macrophage-induced senescence.

To determine if NO• alone could induce cellular senescence, normal human fibroblasts were exposed to clinically relevant levels of NO• and examined for SA-βgal activity. To achieve target steady state levels of 4.5 nM, 15 nM and 50 nM NO•, fibroblasts were incubated with 0.9 μM, 3 μM and 10 μM of the NO• donor Spermine NONOate (Sper/NO•). These doses were chosen because they are consistent with known levels of steady state NO• secreted by macrophages in vitro [35,36] and levels of NO• detected in ulcerative colitis [37]. NO• concentrations at or below 50 nM are below the limit of detection for our NO• gas analyzer. To confirm that Sper/NO• was producing NO• levels near our target concentration, we measured NO• produced by 100 μM Sper/NO• (expected concentration of 500 nM NO•) and found steady state levels of 380 nM NO• at 4 hours (Figure S7; SD ±35 nM; n = 3), similar to the expected concentrations calculated from our previously published data [29]. Treatment with 3 μM and 10 μM, but not 0.9 μM, Sper/NO• induced enlarged SA-βgal positive cells ($P<0.0001$; Figure 3C; Figure S6). Thus, levels of

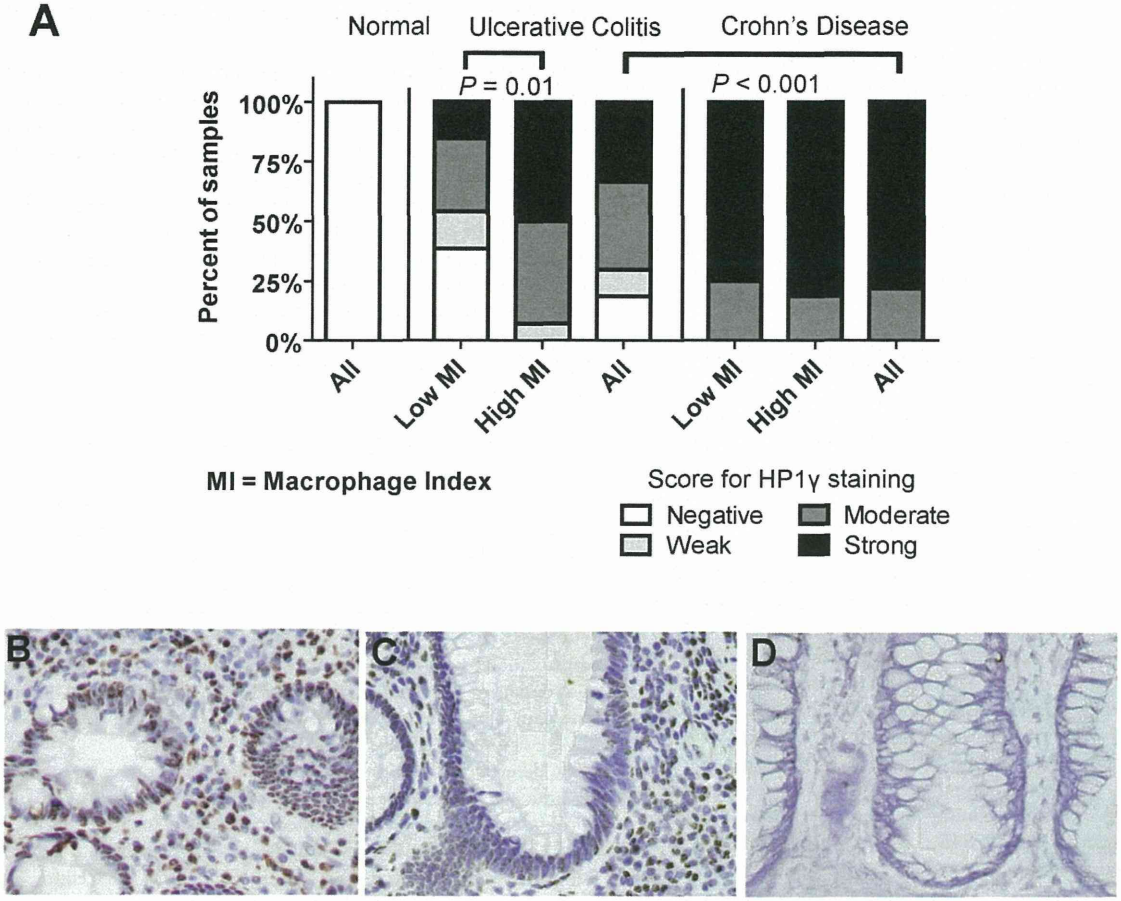

Figure 1. Senescence is induced in inflammatory bowel disease colons in association with infiltrating macrophages. Senescent epithelial cells were identified by HP1γ immunohistochemistry. Categorical scores reflecting intensity and distribution are shown as negative, weak, moderate, and strong. A) Colons from normal patients were negative for senescence-associated HP1γ. Ulcerative colitis and Crohn's disease colonic epithelial cells were positive for HP1γ. Crohn's disease colons had a greater percentage of HP1γ positive cells than ulcerative colitis colons ($P<0.001$). HP1γ was associated with high macrophage index ($P=0.01$) in ulcerative colitis colons, but no such difference was observed within Crohn's disease. B) A representative picture of a Crohn's colitis crypt with strong HP1γ, C) a representative picture of ulcerative colitis crypt with weak staining, and D) a representative picture of normal autopsy tissue with negative staining. All are shown at 400× magnification. Epithelial and stromal HP1γ positive staining cells are shown in brown, with blue-purple hematoxylin counter stain in surrounding cells.
doi:10.1371/journal.pone.0044156.g001

NO• that are physiologically relevant to IBD induce senescence in a dose-dependent manner.

To determine if DDR is upregulated in cells induced into senescence by NO•, we performed immunofluorescence for γH2A.X in MRC5 cells treated with 10 μM Sper/NO•. Indeed, Sper/NO• treated cells showed increased levels of γH2A.X foci, compared to untreated control cells (Figure S8.).

Higher Levels of NOS2 Expression in CD Correlates with Higher Levels of Senescence-associated HP1γ

Macrophages were associated with senescence in epithelial cells in UC, but thus far we could not identify a driver of senescence in CD. Based on our *in vitro* studies that identified NO• as an inducer or senescence, we hypothesized that NO•, secreted by macrophages and produced by epithelial cells themselves may modulate senescence. To study this model of extracellular and intracellular-induced senescence, IHC for NOS2 was performed on tissue. Significantly more epithelial cells were positive for NOS2 in CD than in UC (Figure 4; $P=0.0017$) while no significant difference was observed comparing stromal cells of CD and UC. Increased levels of epithelial NOS2 in CD were consistent with an increase in senescence-associated HP1γ in CD compared to UC (Figure 1A). We were not able to stratify CD tissues to investigate if epithelial cell NOS2 expression correlated with senescence because all CD tissues had high senescence, possibly due to the combined effects of NO• from macrophages and intracellular NO• from epithelial cells. There are no primary epithelial cells of a colonic origin to test our proposal that NO• from epithelial cells is directly related to senescence *in vitro*. We introduce the hypothesis that intracellular (epithelial) NO• may be involved in senescence in CD, and this may be tested should appropriate model systems become available.

MicroRNAs are Associated with NOS2 and Senescence

After establishing that macrophages are associated with senescence in UC, and directly induce senescence in an NO•-dependent fashion *in vitro*, we performed microRNA microarray expression analysis on RNA extracted from both UC and CD tissues to identify candidate microRNAs which may have a role in

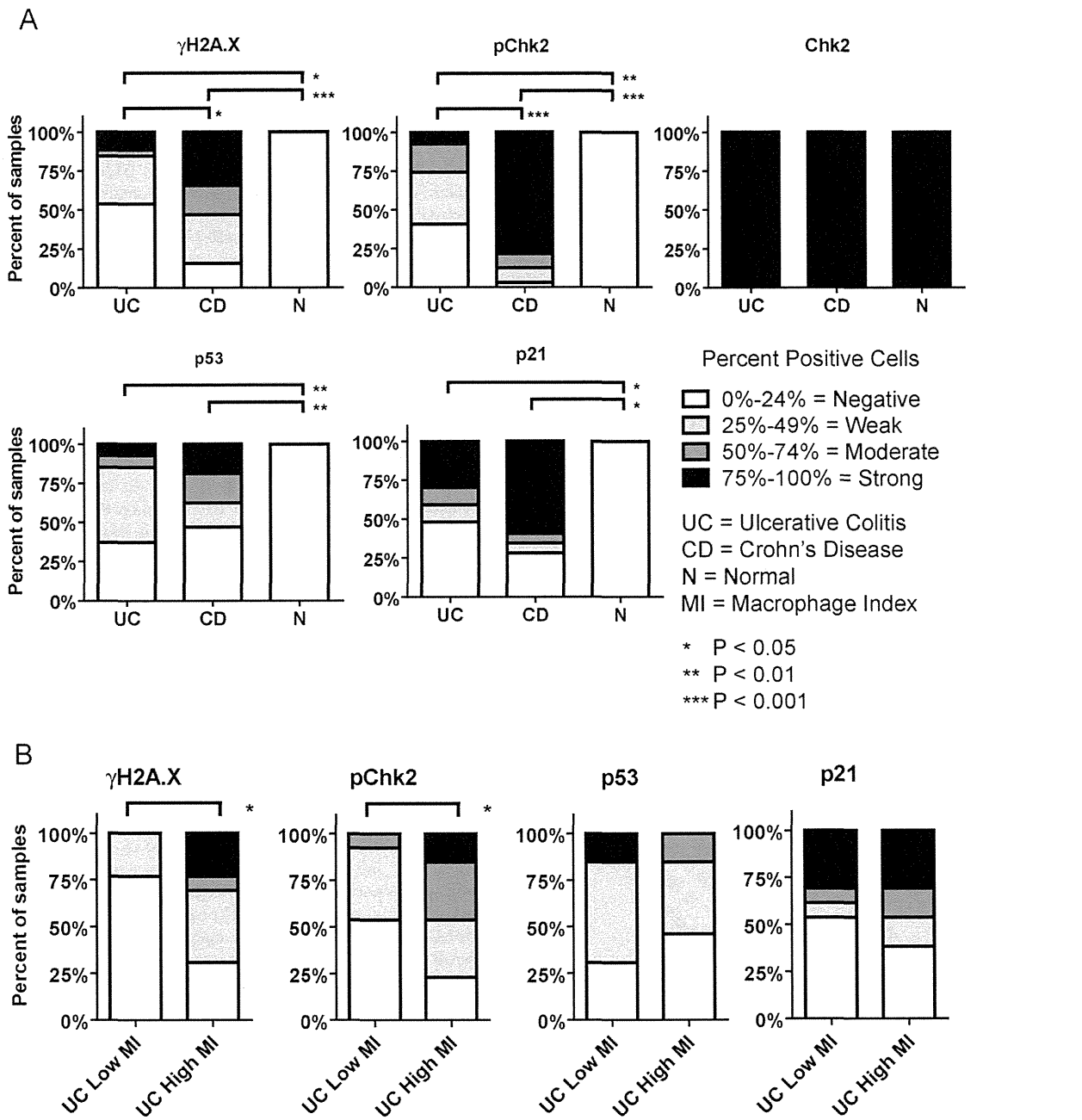

Figure 2. DNA damage response pathway and p21 are upregulated in inflammatory bowel disease and the DNA Damage response pathway is associated with high macrophage infiltration in ulcerative colitis. (A) Normal, ulcerative colitis, and Crohn's disease colons were analyzed by immunostaining to determine the percent of positive epithelial cells for γ-H2A.X, phospho-Chk2, Chk2, p53 and p21. Data is shown by the percent of total samples with 0–24%, 25–49%, 50–74%, and 75–100% cell positivity. Normal colonic epithelial cells had low, or 0–24% cell positivity, for all markers. Both Crohn's disease and ulcerative colitis colons had increased levels of γ-H2A.X ($P<0.001$; $P<0.05$), phospho-Chk2 ($P<0.01$; $P<0.001$), p53 ($P<0.01$) and p21 ($P<0.05$) compared to normal colon. Tissues from Crohn's disease patients showed higher levels of γH2A.X ($P<0.05$), phospho-Chk2 ($P<0.001$) than in ulcerative colitis. No differences were detected in levels of total Chk2 between ulcerative colitis, Crohn's disease, and normal colons, as expected. (B) Analysis of γH2A.X, phospho-Chk2, p53, and p21 in ulcerative colitis colonic epithelial cells was stratified by macrophage infiltration index to determine if macrophage infiltration in the lamina propria was associated with induction of the DNA damage response pathway and p21 activation. Colons with macrophage numbers above the median were defined as having high macrophage index, while those with macrophage numbers below the median were defined as having low macrophage index (i.e., low cellular densities). High macrophage index was associated with increased γH2A.X ($P=0.031$) and phospho-Chk2 ($P=0.014$). No significant differences were observed for p53 and p21 with respect to macrophage index.
doi:10.1371/journal.pone.0044156.g002

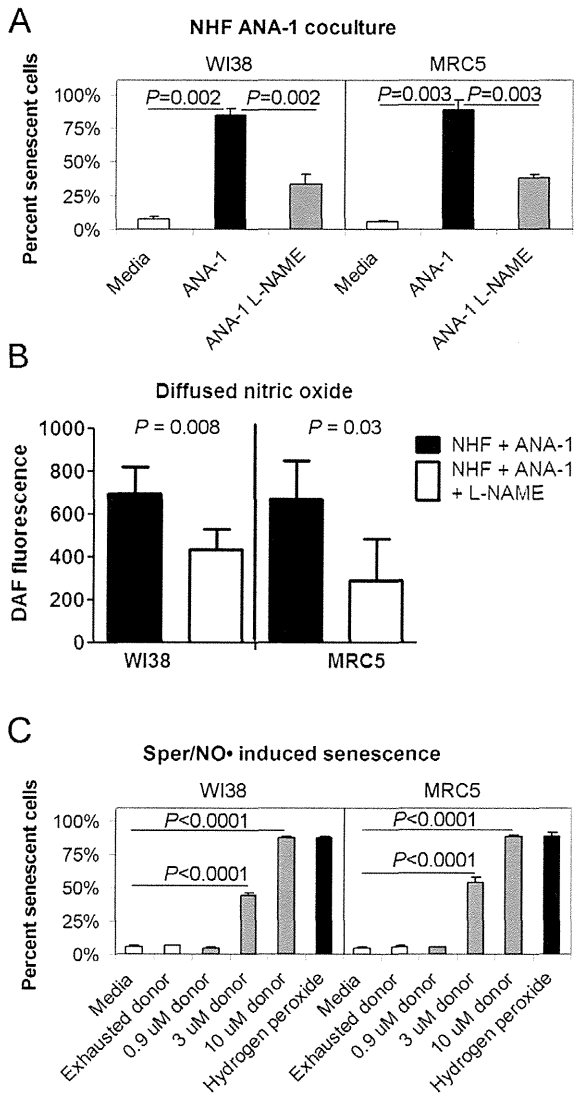

Figure 3. Senescence is induced by either macrophages or NO• in primary normal human fibroblasts in culture. Normal human fibroblasts (WI38 and MRC5) were grown in coculture with murine macrophages (ANA-1), or with the NO• donor spermine NONOate (Sper/NO•). Senescence-associated β-galactosidase activity was used to determine to the percent of senescent fibroblasts divided by the number of total fibroblasts. Results are shown from three experiments, with each experiment done in triplicate. (A) Normal human fibroblasts were cocultured with macrophages, with and without the NO• synthase inhibitor L-NAME (500 μM). Macrophages induced senescence in WI38 and MRC5 cells. Senescence was partially abrogated by L-NAME in WI38 and MRC5 cells. (B) The NO• synthase inhibitor L-NAME reduces diffused NO• in media of cocultures comprised of normal human fibroblasts (WI38 or MRC5) and macrophages (ANA-1). 100 μl of media from three separate cocultures was aliquoted with 100 μL of 5 μM of DAF in 96-well plates. Plates were read for DAF-fluorescence as an indicator of NO•. Addition of the NO• inhibitor L-NAME resulted in decreased levels of NO• in both WI38 ($P=0.008$) and MRC5 ($P=0.03$) cells. Fluorescence measurements from cocultures were normalized by subtracting the DAF fluorescence measured in media from wells with fibroblasts only. (C) Fibroblasts were dosed with 0.09 μM, 3 μM and 10 μM Sper/NO•, Sper/NO• that was previously incubated in media with sodium hydroxide (vehicle) for 48 hours (exhausted donor), and media alone (negative control) overnight (16 hrs). These concentrations were selected to achieve steady state concentrations of 4.5 nM, 15 nM and 50 nM NO• respectively. 10 μM and 3 μM Sper/NO• induced significant levels of senescence ($P<0.0001$). Exhausted Sper/NO• (negative control) and 0.09 μM Sper/NO• did not induce significant levels of senescence when compared to media alone. Hydrogen peroxide (200 μM; 2 hrs) was used as a positive control.
doi:10.1371/journal.pone.0044156.g003

senescence. We measured the expression of NOS2 and the macrophage marker, CD68 by qRT-PCR and analyzed associations between these and microRNA expression levels. We identified 6 microRNAs (miR-21, miR-17, miR-146a, miR-126, miR-223 and miR-221) that were associated with NOS2 expression ($P<0.001$, FDR <5%) indicating that these microRNAs are potentially involved in NO• associated senescence (Figure 5, Table S2). While no microRNAs were associated with CD68 expression at the stringent statistical cutoff of $P<0.001$, a more lenient cutoff identified 5 microRNAs that were associated with CD68 ($P<0.05$), including miR-21, providing evidence that miR-21 may be involved in both macrophage and NOS2 induced senescence.

Colon adenomas are premalignant lesions in which high levels of cellular senescence serves as a barrier to a malignant transformation [12,38]. In order to identify microRNAs whose expression is associated with cellular senescence in multiple disease states, we examined microRNAs expression patterns in senescent adenomas to compare to senescent-associated microRNAs from UC and CD. As expected, adenomas expressed high levels of senescence-associated HP1γ (Figure S3E) and we previously have shown that these adenomas are positive for SA-βgal [39]. This confirms high levels of cellular senescence in these tissues. We next performed microRNA microarray profiling of colonic adenomas and paired normal tissue, and compared these results with our findings in IBD. Among the 31 microRNAs altered in adenomas (Figure 5, Table S3), miR-21 had the highest fold change increase in adenomas, consistent with our previous qRT-PCR data on miR-21 in adenomas [40]. MiR-21 was the only microRNA that was associated with both NOS2 and CD68 in IBD; thus miR-21 is commonly associated with macrophages linked to senescence in IBD and *in vitro*, and NO• which induces senescence *in vitro*. We have previously reported that miR-21 expression is associated with NOS2 expression in colon cancer [41] providing more confidence that this association is relevant. This suggests a potential role for this microRNA in NO• and inflammation-associated senescence, and future investigations will focus on the possible role of miR-21 *in vivo*, and mechanistic experiments *in vitro* to show direct effects that cannot be tested in human tissue. Interestingly, miR-17 was commonly altered in adenomas and associated with NOS2 in IBD while miR-181b was altered in adenomas and associated with CD68.

Conclusions

Cellular senescence is one of the many links between aging and cancer, and may occur through several mechanisms including telomere dysfunction and oncogenic stress [42]. UC has been theorized to be a disease of cellular aging, based on evidence of telomere attrition and chromosomal instability [10,43]. We found that senescence-associated HP1γ expression in colonic epithelia was increased in UC colons in association with a high number of macrophages. This association is consistent with the hypothesis that macrophages may directly or indirectly induce cellular senescence in adjacent epithelial cells, which we observed *in vitro*. Our findings suggest that in addition to cell intrinsic mechanisms such as replicative telomere shortening, microenvironmental cues such as infiltrating immune cells and their derived factors may

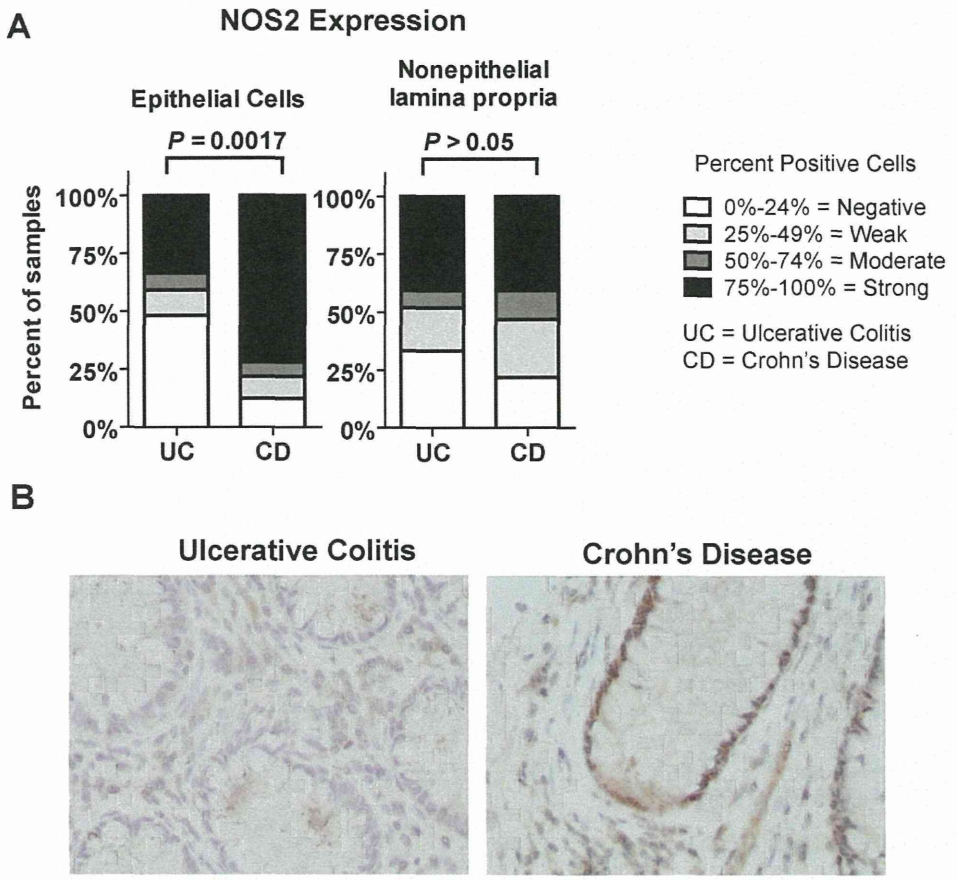

Figure 4. Epithelial cells in Crohn's disease colon show higher levels of anti-NOS2 immunoreactivity than epithelial cells in ulcerative colitis colon. Immunohistochemistry for NOS2 was performed as a possible indicator of NO● produced in the colon of ulcerative colitis and Crohn's disease patients. (A) Colonic epithelial cells had higher NOS2 expression in ulcerative colitis than Crohn's disease ($P = 0.0013$) colons as shown by the percent of samples with positive cells while there was no significant difference in NOS2 expressing cells in the lamina propria. (B) Representative pictures show an ulcerative colitis section with low (0–24% positive) epithelial NOS2, and a Crohn's disease section with high (75–100% positive) epithelial NOS2.
doi:10.1371/journal.pone.0044156.g004

regulate epithelial cell senescence in cancer-prone lesions. This is consistent with a recent report associating high levels of infiltrating lymphocytes with telomere shortening and senescence in UC [44]. Stromal senescent fibroblasts can also secrete proinflammatory cytokines, e.g., IL-6, IL-8 and Gro-α [45] that can contribute to IBD, consistent with our observations.

High macrophage infiltration was associated with increases in the DDR sensor molecule γH2A.X, an indicator of active DNA damage response signaling by upstream DDR kinases including ATM and ATR [46,47], and phosphorylation of downstream stress response protein Chk2 in colonic epithelial cells of inflamed, cancer-prone tissue of UC patients. The increased level of γ-H2A.X in UC colon, when compared to normal colon, is consistent with a previous report [10] and suggests that DDR may lead to cellular senescence in a proinflammatory environment. It is not clear if the DDR response associated with macrophages *in vivo*, and induced by NO• *in vitro*, is pro- or anti-carcinogenic, but DDR has previously been hypothesized to be an anti-cancer barrier [11]. It is possible that macrophages and/or NO• induce the DDR pathway leading to cellular senescence, and limiting proliferation of cells as a barrier to cancer. Alternatively, senescent cells in the microenvironment may themselves be procarcinogenic by secreting cytokines including IL-6, IL-8, IL-1α and IL-1β [38,48].

Our *in vitro* data suggest that macrophages induce cellular senescence in a NO• dependent manner. Macrophages or clinically relevant concentrations of NO• induce cellular senescence in normal human fibroblasts and the NO• synthase inhibitor L-NAME proportionally reduced both NO• and senescence. L-NAME is often considered a nonselective NO• synthase inhibitor, but it has been previously shown to more efficiently block NO• production from NOS3. NOS3 is known to be important in the regulation of NOS2 expression [49], thus we hypothesize that L-NAME may decrease the amount of NO• by inhibiting NOS3 activity and down regulating NOS2 expression. This may be especially relevant at the low levels of steady state NO• (50–100 nmol) expected with 10 μM of Sper/NO• [50]. NO• has been implicated in the activation of the DDR pathway in cell lines and primary cells of patients with Barrett's esophagus. Specifically, NO• donor MAHMA-NONOate induces γH2A.X in Barrett's esophagus non-dysplastic, high-grade dysplastic, and adenocarcinoma cell lines [51]. Interestingly, Dickey *et al.* have shown that NO• induces γH2A.X *in vitro*, and that γH2A.X is induced in unexposed cells adjacent to cells exposed to irradiation [52]. We

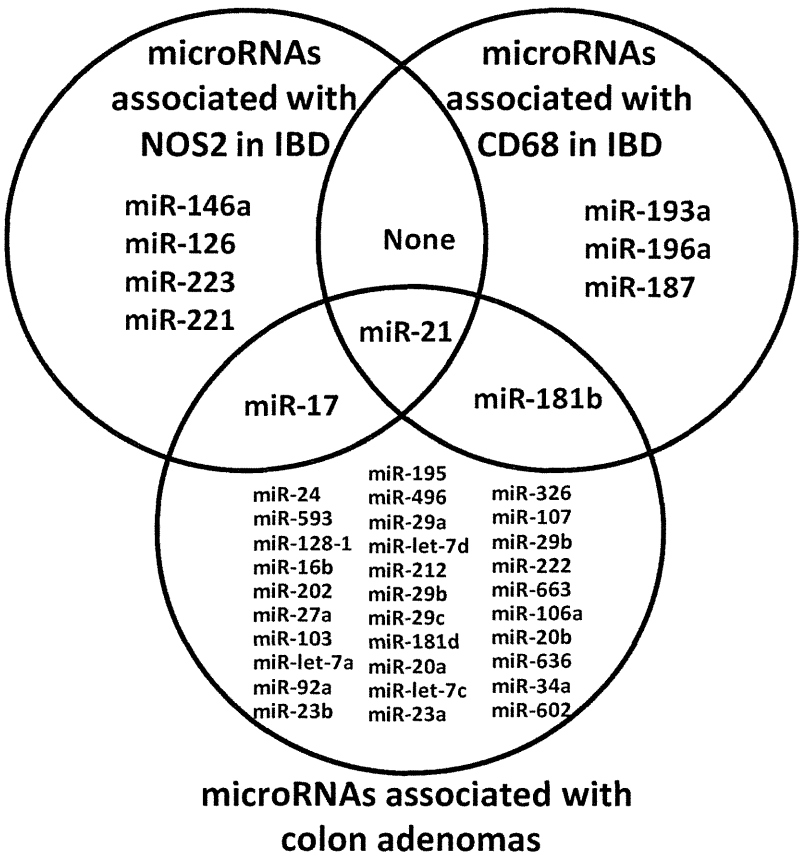

Figure 5. Association of microRNAs with NOS2 and CD68 expression in IBD and microRNAs altered in colon adenomas. The Venn diagram displays microRNAs that were significantly associated with the mRNA expression of NOS2 ($P<0.001$) and CD68 ($P<0.05$) and those microRNAs that are altered in colon adenomas ($P<0.001$) based on microRNA microarray profiling. MiR-21 was found to be associated in all three comparisons suggesting a potential role for this microRNA in senescence.
doi:10.1371/journal.pone.0044156.g005

have also shown that NO• induces γH2A.X in normal human fibroblasts.

NOS2 is increased in colon adenomas [8]; when NOS2 is overexpressed in p53 wild type cells, p53 accumulates and induces a negative feedback loop that down regulates NOS2 expression to decrease nitrosative stress [53]. In contrast, NOS2 overexpression of NOS2 in p53 mutant cells leads to increased angiogenesis and tumorigenicity of human cancer cells as xenografts in immunosuppressed mice [54]. We hypothesize that NOS2 expression in IBD patients with intact and activated p53 serves as a barrier to carcinogenesis, based on the literature and our *in vitro* data that NO• induces senescence and DDR. However, once p53 is inactivated in IBD by mutation [5], nitrosative stress induced by NOS2 may not induce senescence due to loss of p53, and may become procarcinogenic. We plan to investigate these hypotheses should *in vitro* models with primary epithelial cells lines become available.

The miR-146a/b family of microRNAs that are elevated in senescent fibroblasts and thought to modulate senescence through effects on IL-6 and IL-8 [55]. We find that miR-146 expression correlates to NOS2 expression levels in IBD tissues, consistent with a role for miR-146 and NO• in senescence. MiR-21 is an oncogenic microRNA with known roles in inflammation, cell proliferation and tumorigenesis. We found that miR-21 expression is associated with high NOS2 and CD68 expression in UC and CD, as well as colon adenomas. Mir-21 has previously been shown to be increased in active ulcerative colitis [56] and upregulated during DNA damage by hydrogen peroxide and ionizing radiation associated with reactive oxygen species [57]. Inflammatory stimuli, such as *Corynebacterium parvum*-induced inflammation in mice, results in elevated levels of miR-21 [58]. MiR-21 can activate the NO• pathway *in vitro* [59] and miR-21 levels can be regulated by NF-kappaB [60]. Our data suggests that miR-21 may have a role in senescence, although future studies are needed to confirm these results in a second population using a more sensitive assay like RT-PCR, and in *in vitro* studies to show a direct effect. While at first a role in senescence may seem counterintuitive given the oncogenic role of miR-21, other oncogenes, including RAS [61], have roles in oncogene-induced senescence. Interestingly, the RAS pathway has been shown to increase miR-21 expression [62], and NO• can activate the RAS pathway [63]. Therefore, it is possible that in IBD, NO• leads to RAS activation and miR-21 transcription that is in part responsible for senescence in IBD. Future studies should explore if miR-21 is induced by NO• in a RAS-dependent manner and contributes to senescence.

Our study revealed a significance difference in senescence between CD and UC; higher HP1γ-associated senescence was observed in CD than in UC, and may reflect a critical difference between these two chronic inflammatory diseases. Genome wide association studies have shown thus far that some susceptibility loci

are shared by both UC and CD, while others are solely associated with one but not the other disease [64–67]. For example, inflammatory pathways involving IL-23/IL-17 are both implicated in UC and CD, but *NOD2* is associated solely with CD. *NOD2* is required for tolerization of macrophages to bacterial peptides, including ligands for TLR2 and TLR4 [68]. Macrophages from CD Leu1007insC Nod2 homozygote individuals fail to develop tolerance to repeated stimulation with ligands, leading to the production of TNFα, IL-1β, and IL-8 [68]. Mice carrying a similar variant of NOD2 have elevated levels of NF-kappaB and IL-1βin response to MDP [69]. TNFα and IL-1β both contribute to NOS2 expression and NO• production *in vivo* [35], and IL-8 has been shown to be a prosenescent cytokine important to senescence induced by DNA damage [48]. The presence of senescence cells can cause age-related, chronic conditions in addition to inhibiting carcinogenesis [70]. We summarize these data in a model (Figure S9), and propose that regulation of NO• by proinflammatory cytokines contributes to up regulation of the DNA damage response pathway and senescence based on our *in vitro* assays.

Our findings related to inflammatory bowel disease may be applicable to other precancerous states associated with inflammation, and also those associated with oncogenic stress. Macrophages have long been implicated in association with tumors [27], and many questions remain on how immunity is involved in carcinogenesis. Before now, there had been no direct connection established between macrophages or NO• and senescence. Future studies may focus on the modulation of senescence through immune response to improve cancer outcome.

Supporting Information

Figure S1 Antibodies against phospho-Chk2 (Thr68) and Chk2 are specific. HCT116 Chk2−/− and parental Chk2+/+ isogenic cell lines (generously given by the Vogelstein Laboratory) growing in log phase were exposed to 12 Gy of ionizing radiation to induce phospho-Chk2, and harvested 1 hour later. Lysates from Chk2+/+ cells (0 Gy; lane 1, 12 Gy; lane 2), and lysates from Chk2−/− cells (0 Gy; lane 3, 12 Gy; lane 4) are indicated by numbers below each immunoblot. Antibody for (A) phospho-Chk2 (Thr68) used for immunohistochemistry, was determined to be specific by immunoblot, as illustrated by the appropriate sized band detected in irradiated Chk+/+ cells only. (B) Specificity of the Chk2 (clone 273) antibody was confirmed, as shown by the darkest band detected in only Chk2+/+ cells, regardless of irradiation. (C) Additional total Chk2 antibodies (clone 270; Stressgen) and (D) ascites from clone 273 (generously given by Jiri Bartek) were tested to confirm the results. Immunocytochemistry was also performed with (E) phospho-Chk2 (Thr68) and (F) Chk2 (clone 273) antibodies, with similar results. (IR− = O Gy gamma-irradiation, IR+ = 12 Gy gamma-irradiation).
(TIF)

Figure S2 Inflammatory bowel disease colons have increased macrophage infiltration in the lamina propria compared to normal colons. Macrophages were identified with anti-CD68 immunohistochemistry and quantified by enumerating the number of positive brown cells in the lamina propria. Ulcerative colitis and Crohn's disease colons had an increased number of macrophages compared to normal colons (ANOVA, $P=0.02$; Dunn's $P<0.05$ for both comparisons). There was no significant difference in the number of macrophages between colons from ulcerative colitis and Crohn's disease patients.
(TIF)

Figure S3 Senescent cells are detectable by both immunohistochemistry for HP1γ and enzyme activity for senescence associated β-galactosidase in inflammatory bowel disease. A) A representative picture of senescence associated β-galactosidase positivity is shown in frozen sections from ulcerative colitis colon. Colonic epithelial cells showed distinct cytoplasmic blue staining at 100× and B) 400× magnification. (C) Cells of the lamina propria, adjacent to epithelial cells, also stained blue for SAβ-gal activity at 100× and (D) 400× magnification. E) A representative picture of colon adenoma tissue stained for HP1γ.
(TIF)

Figure S4 Examples of immunohistochemistry for DNA damage response and p53-stress response markers. Examples from inflammatory bowel disease colon sections were chosen to emphasize differences reflected in cell counts (represented in Figure 2). Positive cells are indicated by brown nuclear stain (DAB) and negative cells are shown with blue counterstaining (Hematoxylin). Positive staining for γH2A.X, phospho-Chk2, Chk2, p53, and p21 was nuclear. For normal tissues, areas with well-oriented crypts were available, and these are illustrated with the lumen oriented toward the top of the panel. A summary of this data is shown in Figure 2.
(TIF)

Figure S5 Crohn's disease colons show no difference in DNA damage or p53 activation in association with macrophage index. Tissues from Crohn's disease patients were evaluated by immunohistochemistry for γ-H2A.X, phospho-Chk2, total p53 and p21. Staining is not associated with low and high macrophage index ($P>0.05$).
(TIF)

Figure S6 Macrophages and nitric oxide induce senescence in primary human fibroblasts. Representative pictures are shown of positive (blue) and negative (white) cells, indicative of senescence-associated β-galactosidase (SA-βgal) enzyme activity. A) A low density of normal human fibroblasts (MRC5) were cocultured with macrophages (ANA-1) in 6-well plates at a ratio of 3:1, respectively. Cocultures were allowed to grow for 7 days with and without the nitric oxide inhibitor L-NAME (500 μM). Macrophages induced cellular senescence in fibroblasts, as shown by the enlarged, blue, SA-βgal positive cells. L-NAME partially abrogated the induction of senescence in fibroblasts. Cells grown in media only were negative for SA-βgal. (B) Normal human fibroblasts were incubated with 10 μM, 3 μM, and 0.9 μM Spermine NONOate (Sper/NO•) over night (16 hrs). After treatment, the cells were fixed and stained for SA-βgal. Treatment with 10 μM and 3 μM Sper/NO• induced a significant number of enlarged, SA-βgal positive cells, when compared cells grown in media alone (negative control). Treatment with 0.9 μM Sper/NO• did not induce significant levels of SA-βgal positive cells. Hydrogen peroxide (positive control; 200 μM) induced SA-βgal activity.
(TIF)

Figure S7 Steady state nitric oxide was highest at 381 nM at 4 hours, and nitric oxide was decayed by 6 hours. The decay of Spermine NONOate (Sper/NO•) was determined by measuring steady state nitric oxide on a nitric oxide gas analyzer. A 100 μl aliquot of 100 μM of Sper/NO• in serum-free media was aspirated by gas-free syringe into the sampling chamber at 0, 0.75, 1.5, 2, 4, and 6 hour time points.
(TIF)

Figure S8 Nitric oxide induces DNA damage response in primary human fibroblasts in culture. Normal human fibroblasts (MRC5) were incubated with media alone (negative control) or 10 μM Spermine NONOate (donor) and assayed for γH2A.X foci by immunofluorescence as indicated by FITC (green) fluorescence. DAPI (purple blue) was used to identify nuclei, and this image was overlaid with FITC top create a composite. (A, C, E,) Cells grown in media alone were negative for γH2A.X.foci at 400× magnification. (G) Enlargement of a single cell treated with media alone (indicated by the red box in panel C) shows that there is very little FITC fluorescence for γH2A.X. (B, D, F) Cells treated with donor Sper/NO• became enlarged and failed to divide, leading to a low density of cells. Due to the low cell density, it was difficult to capture multiple cells in one 400× magnification field, thus each panel is a composite of four pictures of one single cell each. Each cell shows positive FITC fluorescence for γH2A.X foci. (H) Enlargement of a single cell treated with Sper/NO• (indicated by the red box in panel D) shows distinct focal fluorescence. Panels are shown at 400× magnification except for γH2A.X high magnification panels (G, H), which show an enlarged section (red rectangle) from the γH2A.X panels (C, D).
(TIF)

Figure S9 Proposed model of DNA damage response and senescence resulting from a polymorphism in NOD2/CARD 15 carried by Crohn's disease patients. Previous studies have illustrated that a polymorphism in NOD2 carried by Crohn's disease patients results in the loss of tolerization to bacterial peptide, including TLR2 and TLR4 ligands upon restimulation. [68] This may result in the production of NF-κB and proinflammatory cytokines that are part of a chronic inflammatory response. [69] Cytokines IL-1β and TNF-α can lead to the induction of NOS2 to secrete nitric oxide. [35] Our data suggest that nitric oxide may induce DNA damage and result in cellular senescence.
(TIF)

Table S1 Characteristics of the study populations. [1]CHTN, Cooperative Human Tissue Network.
(XLSX)

Table S2 MicroRNAs are associated with NOS2 and CD68 expression in Ulcerative Colitis (UC) and Crohn's Disease (CD) tissues. NOS2 and CD68 expression levels were dichotomized based on median expression levels. Class comparison analyses identified microRNAs that were differentially expressed when comparing high vs low expressing groups for NOS2 and CD68. FDR, False discovery rate.
(XLSX)

Table S3 MicroRNAs that are altered in colon adenomas compared to adjacent nonadenoma tissue. Class comparison analyses identified microRNAs that were differentially expressed in colon adenomas. FDR, False discovery rate.
(XLSX)

Materials and Methods S1 These are methods that describe the protocols for immunohistochemical anaylsis, coculture and cell culture studies, statistical analysis, senescence-associated β-galactosidase studies, nitric oxide quantification, immunofluorescence, RNA isolation, microRNA profiling and qRTPCR.
(DOC)

Acknowledgments

We acknowledge Dr. Krista Zanetti for her advice on statistics, Dr. Tia Bobo for her technical help, and Dr. Sharon Pine and Dr. Stefan Ambs for thoughtful discussions.

Author Contributions

Conceived and designed the experiments: JJS AJS LAR IH AIR SPH GNW DAW CCH. Performed the experiments: JJS AJS LAR MAK AIR EDB. Analyzed the data: JJS AJS HGY LAR IH AIR SPH AG LJH J. Bartkova J. Bartek GNW DAW CCH. Contributed reagents/materials/analysis tools: LAR DAW J. Bartkova J. Bartek. Wrote the paper: JJS AJS AIR GNW DAW CCH.

References

1. Loftus EV Jr (2004) Clinical epidemiology of inflammatory bowel disease: Incidence, prevalence, and environmental influences. Gastroenterology 126: 1504–1517.
2. Ekbom A, Helmick C, Zack M, Adami HO (1990) Ulcerative colitis and colorectal cancer. A population-based study. N Engl J Med 323: 1228–1233.
3. Nair J, Gansauge F, Beger H, Dolara P, Winde G, et al. (2006) Increased etheno-DNA adducts in affected tissues of patients suffering from Crohn's disease, ulcerative colitis, and chronic pancreatitis. Antioxid Redox Signal 8: 1003–1010.
4. Hofseth LJ, Khan MA, Ambrose M, Nikolayeva O, Xu-Welliver M, et al. (2003) The adaptive imbalance in base excision-repair enzymes generates microsatellite instability in chronic inflammation. J Clin Invest 112: 1887–1894.
5. Hussain SP, Amstad P, Raja K, Ambs S, Nagashima M, et al. (2000) Increased p53 mutation load in noncancerous colon tissue from ulcerative colitis: a cancer-prone chronic inflammatory disease. Cancer Res 60: 3333–3337.
6. Salk JJ, Salipante SJ, Risques RA, Crispin DA, Li L, et al. (2009) Clonal expansions in ulcerative colitis identify patients with neoplasia. Proc Natl Acad Sci U S A.
7. Hofseth LJ, Saito S, Hussain SP, Espey MG, Miranda KM, et al. (2003) Nitric oxide-induced cellular stress and p53 activation in chronic inflammation. Proc Natl Acad Sci U S A 100: 143–148.
8. Ambs S, Bennett WP, Merriam WG, Ogunfusika MO, Oser SM, et al. (1999) Relationship between p53 mutations and inducible nitric oxide synthase expression in human colorectal cancer. J Natl Cancer Inst 91: 86–88.
9. Risques RA, Lai LA, Himmetoglu C, Ebaee A, Li L, et al. (2011) Ulcerative colitis-associated colorectal cancer arises in a field of short telomeres, senescence, and inflammation. Cancer Res 71: 1669–1679. 0008-5472.CAN-10-1966 [pii];10.1158/0008-5472.CAN-10-1966 [doi].
10. Risques RA, Lai LA, Brentnall TA, Li L, Feng Z, et al. (2008) Ulcerative colitis is a disease of accelerated colon aging: evidence from telomere attrition and DNA damage. Gastroenterology 135: 410–418.
11. Bartkova J, Horejsi Z, Koed K, Kramer A, Tort F, et al. (2005) DNA damage response as a candidate anti-cancer barrier in early human tumorigenesis. Nature 434: 864–870.
12. Bartkova J, Rezaei N, Liontos M, Karakaidos P, Kletsas D, et al. (2006) Oncogene-induced senescence is part of the tumorigenesis barrier imposed by DNA damage checkpoints. Nature 444: 633–637.
13. Jones CJ, Kipling D, Morris M, Hepburn P, Skinner J, et al. (2000) Evidence for a telomere-independent "clock" limiting RAS oncogene-driven proliferation of human thyroid epithelial cells. Mol Cell Biol 20: 5690–5699.
14. Campisi J, Yaswen P (2009) Aging and cancer cell biology, 2009. Aging Cell 8: 221–225.
15. Binet R, Ythier D, Robles AI, Collado M, Larrieu D, et al. (2009) WNT16B is a new marker of cellular senescence that regulates p53 activity and the phosphoinositide 3-kinase/AKT pathway. Cancer Res 69: 9183–9191.
16. Serrano M, Lin AW, McCurrach ME, Beach D, Lowe SW (1997) Oncogenic ras provokes premature cell senescence associated with accumulation of p53 and p16INK4a. Cell 88: 593–602.
17. Narita M, Nunez S, Heard E, Narita M, Lin AW, et al. (2003) Rb-mediated heterochromatin formation and silencing of E2F target genes during cellular senescence. Cell 113: 703–716. S009286740300401X [pii].
18. Xue W, Zender L, Miething C, Dickins RA, Hernando E, et al. (2007) Senescence and tumour clearance is triggered by p53 restoration in murine liver carcinomas. Nature 445: 656–660.
19. Schmitt CA, Fridman JS, Yang M, Lee S, Baranov E, et al. (2002) A senescence program controlled by p53 and p16INK4a contributes to the outcome of cancer therapy. Cell 109: 335–346.
20. Di Micco R, Fumagalli M, Cicalese A, Piccinin S, Gasparini P, et al. (2006) Oncogene-induced senescence is a DNA damage response triggered by DNA hyper-replication. Nature 444: 638–642.
21. Rai P, Onder TT, Young JJ, McFaline JL, Pang B, et al. (2009) Continuous elimination of oxidized nucleotides is necessary to prevent rapid onset of cellular senescence. Proc Natl Acad Sci U S A 106: 169–174.